Journal of Asian Earth Sciences 42 (2011) 191–207

Contents lists available at ScienceDirect

Journal of Asian Earth Sciences

journal homepage: www.elsevier.com/locate/jseaes

Geochemical diversity in oceanic basalts hosted by the Zasur'ya accretionary complex, NW Russian Altai, Central Asia: Implications from trace elements and Nd isotopes

I.Yu. Safonova [a,b,*], N.V. Sennikov [c], T. Komiya [d], Y.V. Bychkova [e], E.V. Kurganskaya [a]

[a] Sobolev Institute of Geology and Mineralogy SB RAS, Koptyuga ave. 3, Novosibirsk 630090, Russia
[b] Korean Institute of Geoscience and Mineral Resources (KIGAM), 92 Gwahang-no, Daejeon 305-350, South Korea
[c] Trofimuk Institute of Petroleum Geology and Geophysics SB RAS, Koptyuga ave. 3, Novosibirsk 630090, Russia
[d] The University of Tokyo, 3-8-1 Komaba, Meguro, Tokyo 153-8902, Japan
[e] Vernadsky Institute of Geochemistry and Analytical Chemistry RAS, Kosygina 19, Moscow 19991, Russia

ARTICLE INFO

Article history:
Available online 1 March 2011

Keywords:
Central Asian Orogenic Belt
Late Cambrian–Early Ordovician
Paleo-Asian Ocean
Oceanic island
Oceanic floor
Mantle plume

ABSTRACT

Diverse types of Late Cambrian–Early Ordovician basalts are present as tectonic sheets and fragments in the Early–Middle Paleozoic Charysh-Terekta suture-shear zone of NE Russian Altai. La and Nb depleted, transitional and enriched basalts coexist within this geological structure. Mg# varies from 56 to 20 over a relatively narrow range of SiO_2 (46–52 wt.%). Iron, Zr, Nb, Y, LREE Ti, Cr, Ni and Th variably decrease with Mg#. Depleted tholeiitic basalts have weakly to undepleted LREE (La/Sm_n = 0.6–1.0), weakly fractionated HREE patterns (Gd/Yb_n = 1.1–1.3), relatively high ε_{Nd} (7.7–10.3) and negative Nb and Th anomalies relative to La (Nb/La_{pm} = 0.37–0.8, Th/La_{pm} = 0.4–0.85). Transitional basalts have moderately fractionated REE (La/Sm_n = 1.6–2.0, Gd/Yb_n = 1.3–2.4), medium ε_{Nd} (5.6–5.7) and positive Nb and negative Th anomalies relative to La (Nb/La_{pm} = 1.2–1.6, Th/La_{pm} = 0.7–0.9). Enriched basalts are the prevalent volcanic rock type characterized by LREE-enriched patterns with fractionated HREE (La/Sm_n = 1.9–4.7, Gd/Yb_n = 1.5–2.5), low ε_{Nd} (2.6–3.3), positive Nb and zero to positive Th anomalies (Nb/La_{pm} = 1.0–1.8, Th/La_{pm} = 0.6–1.15). Mantle melting processes, crustal contamination, or fractional crystallization can be ruled out as the main cause of the anomalies except for the moderate effect of alteration and metamorphism on the major-element composition of basalts. The enriched basalts show stronger REE fractionation (La/Yb_n = 6–9), higher positive Nb anomalies, like Phanerozoic HIMU ocean island basalts, than the transitional counterparts (La/Yb_n = 3–4), and also higher Al_2O_3 contents with convex-up trace-element patterns through Th–Nb–La. Both varieties have higher Zr/Hf ratios than depleted basalts and ε_{Nd} values close to those in HIMU. The LREE-depleted basalts are interpreted to have been a mid-oceanic ridge, whereas the transitional and LREE-enriched basalts – a chain of oceanic islands derived from a heterogeneous multicomponent plume tapping the moving oceanic lithosphere. The oceanic islands were fragmented in the accretionary complex and tectonically mixed with underlying MOR tholeiites.

1. Introduction

In recent years, numerous oceanic crust fragments have been found and identified in accretionary complexes of different ages recognized within the Altai-Sayan foldbelt – a north-western part of the Central Asian Orogenic Belt (e.g., Buslov et al., 2001, 2004a; Dobretsov et al., 2004; Safonova et al., 2004, 2008; Ota et al., 2007; Xiao et al., 2010; Wong et al., 2010). Nevertheless, the fragments of ophiolites, oceanic islands and seamounts are generally less common in foldbelts than those of island arcs that may be explained by their smaller volume and poor identification in structures comprising numerous tectonically mixed sedimentary and basaltic-sedimentary terranes (Safonova, 2009). The ophiolites and oceanic islands/seamounts, the fragments of which have been found in Altai-Sayan, were formed in the Paleo-Asian Ocean (PAO). The PAO opened in the Late Neoproterozoic due to the breakup of the Rodinia supercontinent (Maruyama et al., 2007) and existed until the Early Carboniferous (e.g., Zonenshain et al., 1990; Dobretsov et al., 1995; Buslov et al., 2001). Oceanic subduction resulted in the accretion of paleoislands and the underlying oceanic lithosphere to the island arcs bounding the PAO and then

* Corresponding author at: Sobolev Institute of Geology and Mineralogy SB RAS, Koptyuga ave. 3, Novosibirsk 630090, Russia. Tel.: +7 383 3356452; fax: +7 383 3333414.
E-mail address: inna@uiggm.nsc.ru (I.Yu. Safonova).

1367-9120/$ - see front matter © 2011 Elsevier Ltd. All rights reserved.
doi:10.1016/j.jseaes.2011.02.010

to the active continental margin of the Siberian continent. Later oceanic rock units experienced the influence of the processes of collision and subsequent faulting (Buslov et al., 2004b).

The Altai-Sayan foldbelt is a collage of terranes of different ages separated by numerous large-scale thrusts, strike-slip faults and nappes (Buslov et al., 1993, 2004b; Berzin and Dobretsov, 1994; Xiao et al., 2010). The terranes are classified mainly based on Vendian–Cambrian geodynamic units of the Paleo-Asian Ocean. Fig. 1 shows the major structural units that form the Altai-Sayan foldbelt, which is located between the Kazakhstan and Siberian continents (Buslov et al., 2001, 2004a). The tectonic pattern of the western Altai-Sayan comprises the Gondwana-derived Altai-Mongolian terrane, which separated from the margins of East Gondwana (Kurenkov et al., 2002) and later collided with the SW margin of the Siberian continent by a system of strike-slip faults (see Fig. 1 and Buslov et al., 2004b).

However, there are other models for the evolution of this part of the Central Asian Orogenic Belt based on the accretion of oceanic arcs and/or Gondwana-derived continental blocks to the Siberian, Russian, and North China cratons (e.g., Zonenshain et al., 1990; Didenko et al., 1994; Windley et al., 2007; Xiao et al., 2008; Yakubchuk, 2004; Rojas-Agramonte et al., in press) or accumulation of Paleozoic subduction-accretion materials against a few extended magmatic arcs (Sengör and Natal'in, 1996).

The north-western part of Altai-Sayan, Rudny Altai in Russian literature, belongs to a reactivated suture zone (Charysh-Terekta) which extends into the Altai-Mongolian terrane and hosts fragments of the Late Cambrian–Early Ordovician oceanic lithosphere (Fig. 1). Based on geochemically and geochronologically distinct volcanic and sedimentary rocks, tectonically juxtaposed in a tectonic mélange, and regional scale transpressional structural characteristics, Buslov et al. (2000, 2004b) interpreted the late Devonian Charysh-Terekta strike-slip or suture-shear zone as a subduction–accretion complex that formed along an Devonian convergent plate margin as a result of the Late Devonian collision of the Gondwana-derived Altai-Mongolian microcontinent and Siberian continent (Fig. 1; Buslov et al., 2001, 2004a). In this geodynamic framework, based on a very limited amount of geochemical data, tholeiitic and alkaline basalts were previously interpreted as dismembered fragments of the oceanic lithosphere of the PAO formed in mid-oceanic ridge and oceanic island settings (Buslov et al., 2000, 2001; Safonova et al., 2004).

The geochemical characteristics of Paleozoic oceanic basalts are of particular interest for understanding mantle evolution, petrogenesis and geodynamic processes. Besides, the study of oceanic magmatism is very important because it is an integral part of the study of orogenic belts incorporating many commercially valuable mineral deposits. The mutually correlated geochronological and compositional data on ophiolites and intra-plate basalts are necessary for reconstructing the histories of the paleo-oceans and their related accretionary processes, which significantly contributed to the Paleozoic continental growth of Central and East Asia. Last but not least, identification of OIB-type basalts (oceanic island basalts) is important for mantle plume modeling and global geodynamic paleoreconstructions (e.g., Maruyama et al., 1997; Safonova et al., 2009; Zhang et al., 2010).

This paper reviews few already published geochemical data (Sennikov et al., 2003, 2004; Safonova et al., 2004) and presents new high-precision ICP-MS trace element data for compositionally diverse basalts from the Zasur'ya unit or accretionary complex (Late Cambrian–Early Ordovician) of the Charysh-Terekta strike-slip zone located in Rudny Altai (Figs. 1 and 2). We also report first Nd–Sr isotope data for Zasur'ya basalts. Based on these results we attempt to resolve different components in the mantle sources from which the basalts were derived, and address the geodynamic settings of basalt eruption.

2. Geology

The geological structure of the Charysh-Terekta zone comprising the Zasur'ya accretionary complex with oceanic crust

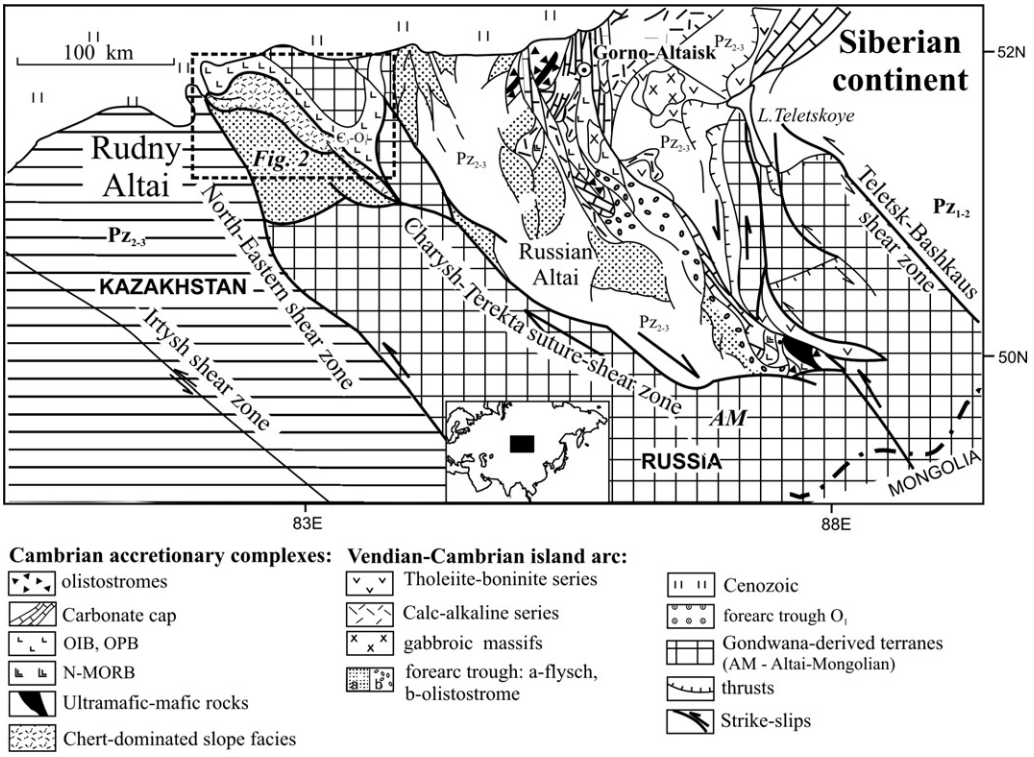

Fig. 1. Regional geology of the western Altay-Sayan foldbelt. NW Gorny Altai is outlined by a dotted rectangle. Modified from (Buslov et al., 2001).

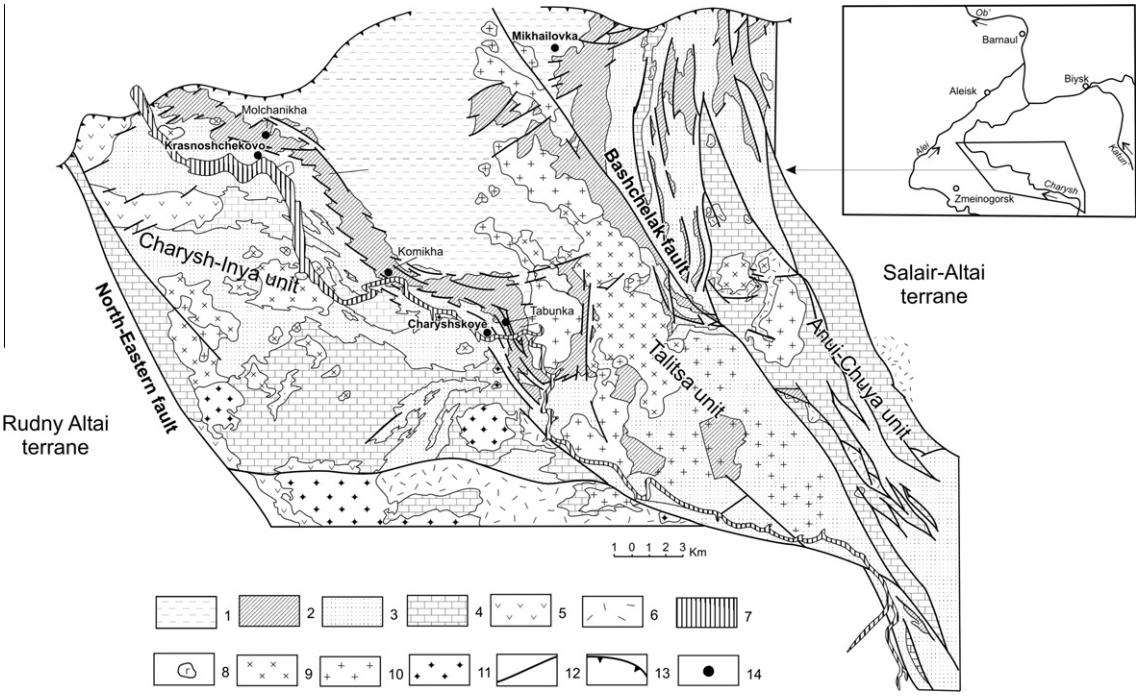

Fig. 2. Tectonic scheme of the Charysh-Terekta strike-slip zone hosting the Zasur'ya AC (modified from Sennikov et al. (2003) and Buslov et al. (2000)). 1 – Cambrian (?) terrigeneous rocks without paleontological constrains; 2 – Late Cambrian–Early Ordovician Zasur'ya Series with oceanic sediments and volcanic rocks; 3 – Ordovician–Silurian terrigeneous-carbonate sediments; 4 – Ordovician–Silurian carbonates; 5, 6 – Devonian volcanogenic-sedimentary rocks with mafic to andesitic (5) and felsic (6) volcanic rocks; 7 – Cenozoic sediments; 8–11 – intrusive rocks: 8 – Devonian gabbroids, 9 – Late Devonian–Early Carboniferous biotite-hornblende I-type granitoids, 10 – Late Devonian–Early Carboniferous A-type granites and leucogranites, 11 – Late Permian–Early Triassic amphibole-biotite S-type granites; 12 – faults; 13 – Altai major thrusts; 14 – location of sites/villages/small rivers.

fragments was discussed in Buslov et al. (1999, 2000) and Safonova et al. (2004). The Charysh-Terekta strike-slip zone in NW Russian Altai extends over a distance of 120–130 km and consists of several deformed structural units (from west to east): Charysh-Inya, Zasur'ya, Talitsa and Anui-Chuya. The structural units which occur as structural sheets and lenses are bounded by the late Carboniferous-Permian North-Eastern and Bashchelak faults (Fig. 2). These units are composed of sandstones, cherts, pillow-lavas and lava flows, volcanoclastics, and gabbro-diabase dikes (Buslov et al., 2000; Safonova et al., 2004).

The Late Cambrian–Early Ordovician Zasur'ya unit or series of the Charysh-Terekta strike-slip zone is of special interest because it comprises several tectonic lenses consisting of terrigenous and oceanic sediments and ophiolites including variolitic or aphyric pillow-lavas, plagioclase and pyroxene–plagioclase porphyritic basalts and their volcaniclastic derivatives, gabbro and gabbro-diabases (Fig. 2). The basalts are associated with the sediments of Oceanic Plate Stratigraphy (OPS; Isozaki et al., 1990) such as pelagic radiolarian/ribbon chert, hemipelagic siliceous shale, mudstone, and other epiclastic slope facies. Biostratigraphy of associated oceanic siliceous sedimentary rocks was reported in Iwata et al. (1997) and Sennikov et al. (2003, 2004).

The breccia-like structure, synsedimentation and asymmetrical folding textural features of the cherts suggest that they represent slope facies of oceanic islands. The Zasur'ya Series or is characterized by a unique combination of terrigenous, volcanic and siliceous units (Fig. 2). The color of the cherts ranges from red to violet and from gray to brown, depending on the degree of alteration by diagenesis and sea-floor-surface redox conditions (Fig. 3A), which is typical of present-day seamount slope sedimentation environments (Jones and Murchey, 1986 and references therein). The silica-rich layers are up to several hundred meters thick with individual siliceous beds of 20–30 meters (Sennikov et al., 2003). The Series consists of three suites: (1) the lower Listvennaya Suite of red and gray siliceous shale, mudstone, chert and basalt (Fig. 3A); (2) the middle Talitskaya Suite chert, siliceous shale, sandstone and siltstone; (3) the upper Marchetinskaya Suite of intercalated red and gray siltstone, siliceous shale and mudstone. No conformable contacts have been found between these three suites: probably the rocks were replaced in respect to each other along strike-slip faults (Buslov et al., 2000). The stratified cherts of the Listvennaya Suite contain Late Cambrian pelagic planktonic conodonts and radiolarians with siliceous skeletons (Iwata et al., 1997; Sennikov et al., 2003).

Samples for geochemical analyses were obtained from the least altered and deformed outcrops of volcanic flows in the Charysh-Terekta zone, along the Molchanikha River (Nos. 96-71, 96-72) and near Krasnoshchyokovo Village (Nos. 97-120-1a, 91-120-3, 97-120-5), along the Tabunka River (Nos. C-997, C-9914, C-9914a, Zas-21/22-07) and Komikha River (Nos. Zas-23/25-07, 95-130) near Charyshskoye Village, and on the left bank of the Slyudyanka river near Mikhailovka Village (Nos. 96-81, Zas-30/31-07; Fig. 2; Table 1).

3. Petrology

Medium to strongly altered volcanic rocks were sampled from the Listvennaya Suite of volcanogenic-sedimentary rocks of the Zasur'ya Series (Figs. 2, 3a; see Section 2). The rock samples collected and analyzed in this study are basaltic lavas, microgabbros and diabases, which display well-preserved original igneous textures in spite of post-magmatic alteration. The basalts are dark gray to green–gray in color and commonly show massive

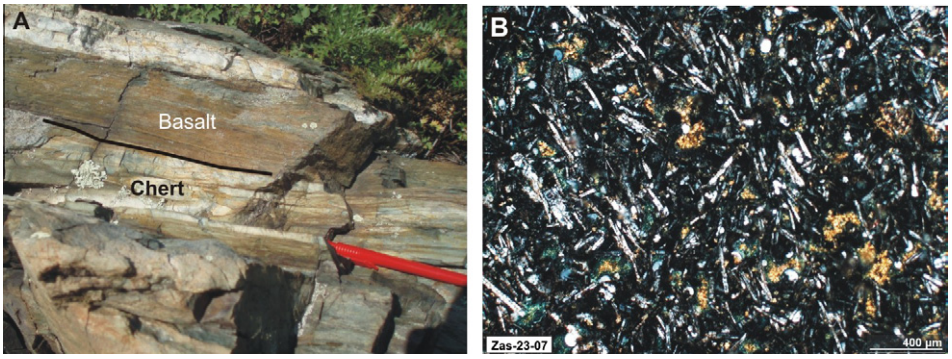

Fig. 3. A – Original/sedimentary field contacts of oceanic light gray to brown chert and basalt. B – typical aphyric basalt (thin-section). (For interpretation of the references to colour in this figure legend, the reader is referred to the web version of this article.)

structure and subporphyritic, porphyritic and ophitic textures (Fig. 3B). The porphyric varieties consist of phenocrysts of altered clinopyroxene and plagioclase up to 1–2 mm in size. The groundmass contains fine-grained plagioclase, pyroxene, Fe–Ti oxides and volcanic glass. Pyroxene phenocrysts and volcanic glass are partly or completely replaced by saussurite, chlorite, calcite, and epidote, and plagioclase by albite. The microgabbros and diabases show various degrees of hydrothermal-metamorphic alteration effects resulting in development of quartz, albite, epidote, chlorite, calcite, hornblende and hematite. The mineral assemblage consists of plagioclase (25–30%), hornblende (50–65%), clinozoisite and epidote (5–10%), opaque mineral, leucoxene and chlorite (up to 5%). The prismatic crystals of light-colored hornblende are partly replaced by leucoxene containing albite-oligoclase (N_g = 1540, N_p = 1535). The opaque minerals are subidiomorphic and xenomorphic Ti-magnetite and idiomorphic magnetite grains.

Our study mainly focuses on the whole rock geochemical characteristics because it was very hard to find fresh grains of olivine, pyroxene and plagioclase and to get pure igneous mineral separates.

4. Analytical methods

This paper presents both original and published geochemical data. Representative samples of metabasalts, microgabbros and diabases were selected for analyses. The rock samples were first split into small chips and soaked in cold 4 N hydrochloric acid for 1 h in order to leach out possible alteration minerals. The rock chips were then ground in an agate mill. Abundances of major-elements in all samples were determined at the Institute of Geology and Mineralogy SB RAS by X-ray fluorescence spectrometry (XRF) using a "Nauchpribor" device. The analytical procedure followed the Russian state analytical standard OST-41-08-212–82 Mingeo SSSR; relative standard deviations (RSD) are within 5%, and totals were within 100 ± 1%. Trace elements in new samples (Zas-21/31-07) were analyzed by inductively coupled plasma mass-spectrometry (ICP-MS) in the Tokyo Institute of Technology (ThermoElemental VG 244 PlasmaQuad 2 LA ICP-MS; on fused glass beads) and in the Institute of Geology and Mineralogy SB RAS (Finnigan Element ICP-MS device; on powdered samples) using the protocols of Jenner et al. (1990). Powdered samples were dissolved using a HF-HNO_3 (2:1) mixture in a screw-top Teflon beaker for 2 days at ~100 °C followed by evaporation to dryness, refluxing in 6 N HCl and drying twice, and then dissolution in 1 N HCl. The procedure was repeated until the powder was completely dissolved. The final solution was evaporated to dryness, refluxing in 6 N HNO_3 and drying three times, and dissolved in 2% HNO_3. Wet chemical procedures were conducted under clean lab conditions. BHVO-1 (Jenner et al., 1990), BCR-1 (Jochum and Nohl, 2008) and JB-3 (Orihashi and Hirata, 2003) were used as international reference materials to estimate precision and accuracy. The analytical errors are estimated as 2–7% for rare earth elements (REE) and high-field strength elements (HFSE).

The obtained analyses were screened for least alteration on the criteria of preservation of igneous textures, petrographic freshness, low losses on ignition (L.O.I.; Table 1), coherent chondrite normalized REE patterns and primitive mantle-normalized multi-element spectra for given igneous suites.

The published trace element data (see footnote to Table 1) were obtained by synchrotron radiation XRF (Ni, V, Rb, Sr, Y, Zr, Nb), atomic absorption (Ni, Ba, Rb, Sr) and instrumental neutron activation analysis – INAA (REE, Hf, Ta, Th, U, Rb, Ba, Cr; Safonova, 2005; Sennikov et al., 2003; Safonova et al., 2004). The synchrotron radiation XRF technique is described in Phedorin et al. (2000). The atomic absorption was performed using a Pye Unicam SP-9 spectrometer following the Russian state analytical standard OST-41-08-205-04. The details of the technique were reported in (Simonova et al., 1987); the analytical error is within 10%. The INAA was performed by using Ge detectors for γ-rays higher that 30 keV and below 2000 keV. All the data are of good quality and well within international standards; the analytical errors on most REE and HFSE were within 5–10% (Safonova, 2005).

Selected elements are normalized to chondrite (n) and primitive mantle (pm) (Sun and McDonough, 1989) such that zero fractionation represents 1 (e.g., primitive mantle Nb/Th_{pm} = 1). Zr/Zr^* and Eu/Eu^* ratios were calculated with respect to the neighboring immobile elements, following the method of Taylor and McLennan (1985). Samples were recalculated to 100% anhydrous for intercomparisons. Mg-numbers (Mg#) were calculated as the molecular ratio of $Mg/(Mg + Fe^{2+})$ assuming 10%Fe^{3+}, which corresponds to low-pressure crystallization conditions for oxygen fugacity of ~FMQ-1.

The isotopic compositions of Sm, Nd, Sr, and Rb were analyzed at the Vernadsky Institute of Geochemistry and Analytical Chemistry RAS using a TRITON mass spectrometer. The concentrations of Rb, Sr, Sm, and Nb were determined by the isotope dilution method. The samples were decomposed in an HF + HNO_3 mixture at a temperature of 200 °C for two days using titanium autoclaves with Teflon inserts. The sample was spiked before decomposition with a mixed ^{85}Rb + ^{84}Sr tracer. The separation of Rb, Sr, and all rare earth elements was carried out by ion exchange chromatography using Teflon columns with 3.5 ml of Dowex 508 resin and 2.3 N HCl as an eluent. Nd and Sm were separated on Eichrom Ln.spec columns by stepwise eluation with 0.5 N and 0.75 N HCl, respectively. The long-term precision of isotopic analysis was controlled using international standards: SRM-87 for Sr and La Jolla for Nd. The obtained

Table 1
Major oxides (wt.%) and trace elements (ppm) in the Zasur'ya basalts.

	1	2	3	4	5	6	7	8	9	10	11	12	13	14	15	16	17	18	19	20	21	22	23
Sample	Zas-21-07	Zas-22-07	97-120-1a	96-81	C-997	C-9912	Ї-2921	E-2921	96-83	C-007-3	C-9914A	97-120-3	97-120-5	95-130	96-71	96-72	B-2921	V-2921	Zas-23-07	Zas-24-07	Zas-25-07	Zas-30-07	Zas-31-07
SiO_2	48.1	47.18	48.93	48.15	47.59	47.96	47.93	48.20	46.44	47.70	46.17	43.98	45.91	46.40	49.05	52.37	46.56	47.13	49.91	45.38	45.67	44.86	44.26
TiO_2	1.95	1.42	1.32	1.96	1.47	1.54	1.56	1.99	2.04	2.14	2.08	4.05	2.79	2.39	2.73	2.71	3.19	2.71	2.72	2.93	3.15	2.53	3.84
Al_2O_3	14.3	14.4	13.7	13.8	14.45	15.7	13.7	16.1	14.4	17.2	14.3	16.6	15.3	18.8	14.1	14.7	19.5	17.8	17.7	17.4	16.5	16.6	15.4
Fe_2O_3	13.8	13.0	9.7	14.2	12.68	11.6	13.9	12.1	12.4	9.5	14.0	14.7	13.2	8.5	16.9	15.4	14.2	11.2	8.3	11.1	11.5	12.2	12.6
MnO	0.19	0.18	0.20	0.26	0.22	0.26	0.21	0.20	0.22	0.21	0.25	0.27	0.18	0.11	0.08	0.14	0.15	0.17	0.19	0.19	0.3	0.19	0.21
MgO	7.12	7.93	8.35	6.99	8.50	7.02	7.45	6.79	8.57	5.74	7.48	4.05	7.72	5.50	2.49	1.97	2.29	7.25	5.28	7.29	6.33	7.77	6.33
CaO	8.87	11.49	9.66	10.9	8.80	8	9.77	8.08	8.20	7.92	8.56	7.24	8.11	8.80	4.70	4.25	3.18	3.59	5.29	7.33	5.44	6.95	8.48
Na_2O	3.3	2.14	2.46	2.14	2.56	4.74	2.27	2.73	2.85	3.20	3.81	3.22	2.50	2.85	4.89	3.15	2.14	3.28	5.9	3.05	5.1	3.93	3.26
K_2O	0.23	0.51	0.41	0.13	0.48	0.69	0.24	0.76	0.92	0.59	0.15	0.22	0.36	0.65	2.82	3.25	5.37	2.16	0.68	0.26	0.14	0.38	0.65
P_2O_5	0.19	0.13	0.18	0.16	0.15	0.21	0.16	0.27	0.20	0.43	0.24	0.48	0.38	0.61	0.72	0.75	0.57	0.47	0.52	0.54	0.56	0.49	0.85
L.O.I.	2.35	1.99	5.06	2.70	2.79	3.02	2.77	2.77	3.44	4.87	2.75	5.02	3.49	4.92	1.94	1.35	2.83	4.15	3.62	4.76	5.52	3.88	3.71
Total	100.4	100.4	100.0	101.3	99.7	100.8	100.0	100.0	99.7	99.4	99.8	99.9	99.9	99.4	100.4	100.0	99.9	99.9	100.1	100.2	100.2	99.8	99.6
Mg#	51	55	63	50	57	55	52	53	58	55	52	36	54	57	23	20	24	56	56	57	52	56	50
Rb	6.0	12.1	10.0	4.0	6.0	3.0	3.0	18.0	13.0	12.0	11.0	11.0	7.0		27.0	40.0	124.0	35.0	17.9	8.9	4.7	12.4	24.0
Sr	202	237	97	230	191	134	144	338	490	747	422	321	425		300	360	135	403	349	391	326	701	1033
Y	37.6	31.9	33.0	40.0	33.5	54.6	34.0	32.0	32.0	34.4	27.6	40.0	42.0		54.0	82.0	45.0	34.0	41.6	44.5	48.6	38.2	57.6
Zr	154	128	84	112	104	157	85	124	160	220	104	239	191		330	565	259	222	479	299	325	328	426
Nb	7.0	4.3	1.0	5.0	5.1	9.5	5.0	21.0	19.0	31.9	30.4	35.0	27.0		54.0	65.0	59.0	50.0	53.3	45.6	57.5	72.4	92.6
Ba	60	61	138	30	66	80	120	382	500	150	386	200	209		320	550	557	905	446	81	68	572	637
La	6.4	4.6	2.9	6.0	5.2	7.3	5.6	12.7	15.0	17.0	12.8	24.9	18.9	42.0	50.0	40.0	33.5	29.8	32.4	28.4	35.2	46.7	54.6
Ce	17.3	12.6	8.90	14.5	13.0	19.0	14.6	27.5	30.0	37.0	24.0	54.0	41.0	77.0	100.0	76.0	70.0	56.5	71.1	64.4	76.3	95.8	115.7
Nd	8.7	7.4	9.5	10.0	10.0	15.0	10.0	16.5	15.0	25.0	16.0	31.0	26.0	24.0	65.0	44.0	38.0	29.0	27.2	25.8	30.9	38.8	40.6
Sm	4.0	3.7	3.2	4.0	3.5	5.2	3.6	4.8	4.5	4.7	4.1	8.6	7.2	5.6	14.0	12.5	9.7	6.8	8.4	8.0	10.3	10.5	13.1
Eu	1.41	1.26	1.11	1.60	1.21	1.61	1.29	1.62	1.9	1.7	1.3	2.88	2.34	2.5	4.1	3.8	2.98	2.24	2.56	2.72	3.28	3.22	4.02
Gd	2.81	2.64	4.10	6.00	4	6.6	4.60	5.1	4.6	3.6	4.3	8.4	8.1	6.3	14		9.1	7	8.65	4.93	5.93	11.0	13.2
Tb	0.80	0.84	0.74	1.05	0.80	1.17	0.83	0.94	0.90	0.70	0.73	1.43	1.29	1.10	2.20	1.80	1.51	1.08	1.43	1.57	1.60	1.45	1.67
Dy	5.04	5.44																	8.30	8.14	9.17	7.32	8.95
Ho	1.06	1.06																	1.41	1.43	1.60	1.31	1.39
Er	2.98	3.01																	4.47	4.46	4.35	3.19	4.53
Tm	0.61	0.57								0.35									0.76	0.69	0.79	0.57	0.97
Yb	2.99	3.21	2.61	4.20	3	5.1	3.20	2.66	2.5	2.7	2.6	2.8	3.9	2.6	7.5	6.8	3.39	2.35	4.57	4.34	4.73	3.49	6.36
Lu	0.5	0.5	0.4	0.6	0.5	0.8	0.5	0.4	0.4	0.4	0.4	0.4	0.5	0.4	1.1	1.1	0.5	0.3	0.6	0.7	0.7	0.5	0.8
Hf	4.6	4.9	2.2	3.2	2.5	4.2	2.3	3.4	3.5	3.4	2.6	6.0	4.7		12.0	12.0	6.4	5.4	11.8	8.3	8.9	8.8	11.2
Ta	0.5	0.3	0.1	0.4	0.3	0.3	0.3	1.1	0.8	1.3	1.3	1.9	1.5		3.0	3.2	3.2	2.6	4.3	3.4	4.1	5.1	7.1
Th	0.5	0.4	0.3	0.3	0.4	0.5	0.4	1.4	0.4	1.6	1.5	2.5	1.6		3.7	4.3	4.5	3.5	4.0	3.5	4.6	5.5	7.5
Ba/Rb	9.9	5.0	13.8	7.5	11.0	26.7	40.0	21.2	38.5	12.5	35.1	18.2	29.9		11.9	13.8	4.5	25.9	24.9	9.2	14.5	46.2	26.6
La/Sm_n	1.0	0.7	0.9	1.0	0.6	0.9	0.9	1.7	2.1	2.3	1.9	1.8	1.6	4.7	2.2	2.0	2.2	2.7	2.2	1.8	2.1	2.8	2.6
Gd/Yb_n	1.3	1.0	1.2	1.2	1.3	1.1	1.0	1.6	1.5	1.1	1.3	2.4	1.7	2.0	1.5	1.4	2.2	2.4	1.7	1.7	1.0	2.5	2.4
La/Yb_n	1.5	0.8	1.0	1.2	0.8	1.2	1.0	3.2	4.1	4.3	3.3	6.0	3.3	11.0	4.5	4.0	6.7	8.6	4.4	4.8	5.1	9.1	8.5
$(Eu/Eu^*)_n$	1.0	1.1	1.0	1.0	0.9	1.0	0.8	1.0	1.3	1.2	0.9	1.0	0.9	1.3	0.9	0.9	1.0	1.0	1.0	1.1	1.2	0.9	0.9
ΣREE	57	49	33	48	41	62	44	72	75	93	66	134	109	162	258	186	169	135	180	163	194	235	280
Al_2O_3/TiO_2	7.3	10.2	10.4	7.0	9.8	6.9	8.8	8.1	7.1	5.1	10.2	4.1	5.5	7.8	5.1	5.4	6.1	6.6	6.5	5.9	5.2	6.6	4.0
Ti/Zr	0.0	0.0	95.2	122.8	0.0	0.0	115.3	108.1	92.6	0.0	0.0		101.0		58.9	34.0	89.6	82.0	0.0	0.0	0.0	0.0	0.0
Zr/Nb	22.0	29.9	84.0	22.4	20.6	16.5	17.0	5.9	8.4	6.9	3.4	6.8	7.1		6.1	8.7	4.4	4.4	9.0	6.6	5.7	4.5	4.6
Zr/Y	4.1	4.0	2.5	2.8	3.1	2.9	2.5	3.9	5.0	6.4	3.8	6.0	4.5		6.1	6.9	5.8	6.5	11.5	6.7	6.7	8.6	7.4
Y/Nb	5.4	7.5	33.0	8.0	6.6	5.7	6.8	1.5	1.7	1.1	0.9	1.1	1.6		1.0	1.3	0.8	0.7	0.8	1.0	0.8	0.5	0.6
Zr/Hf	33.4	26.0	38.2	35.0	41.6	37.4	37.0	36.5	45.7	64.7	40.0	39.8	40.6		27.5	47.1	40.5	41.1	40.5	35.8	36.7	37.2	38.1
Nb/Ta	15.3	16.8	14.3	13.5	17.4	27.9	19.2	18.8	23.8	24.5	23.2	18.7	17.9		18.0	20.3	18.7	18.9	12.4	13.2	13.9	14.1	13.1
Nb/La_{pm}	1.1	0.9	0.8	0.9	1.0	0.9	1.3	1.6	1.2	1.8	2.3	1.4	1.4		1.0	1.6	1.7	1.6	1.8	1.5	1.6	1.5	1.6

(*continued on next page*)

Table 1 (*continued*)

	1	2	3	4	5	6	7	8	9	10	11	12	13	14	15	16	17	18	19	20	21	22	23
Sample	Zas-21-07	Zas-22-07	97-120-1a	96-81	C-997	C-9912	Γ-2921	E-2921	96-83	C-007-3	C-9914A	97-120-3	97-120-5	95-130	96-71	96-72	B-2921	V-2921	Zas-23-07	Zas-24-07	Zas-25-07	Zas-30-07	Zas-31-07
Th/La_{pm}	0.6	0.7	0.4	0.6	0.8	0.6	0.6	0.9	0.9	1.9	0.9	0.8	0.7		0.6	0.9	1.1	0.9	1.1	1.0	1.0	1.0	1.1
Nb/ Th_{pm}	1.7	1.4	2.0	1.5	1.2	1.5	2.3	1.8	1.4	0.9	2.4	1.7	2.0		1.7	1.8	1.6	1.7	1.6	1.5	1.5	1.6	1.5
$(Zr/Zr)^*$	0.7	0.8	0.8	1.0	1.0	0.8	0.8	1.0	0.7	0.7	1.1	1.0	1.0		1.3	0.6	1.0	0.9	0.4	0.7	0.8	0.9	0.8

Columns: 1–7 – depleted basalts (MORB-type); 8–13 – transitional basalts (T-OIB-type); 14–23 – enriched basalts (OIB-type). The previously published data for 5, 6 are from Sennikov et al. (2003)) and for major oxides in 4, 7–9, 13–17 from Safonova et al. (2004).

isotopic ratios are $^{87}Sr/^{86}Sr = 0.710256 \pm 18$ ($N = 21$) and $^{143}Nd/^{144}Nd = 0.511843 \pm 11$ ($N = 19$).

5. Results

5.1. Major and trace element compositions

A part of the whole rock analyses of basaltic rocks from the Zasur'ya AC was reported by Sennikov et al. (2003) and Safonova et al. (2004). Table 1 the chemical data, both new and few previously published, with Fe tabulated as Fe_2O_3. On the basis of their Ba/Rb abundance ratios ranging from 5 to 40 compared to the average oceanic basalt ratio of 11.6 (Hofmann and White, 1982) these rocks have experienced significant post-magmatic mobility of alkali metals. Most samples contain more than 2 wt.% H_2O (based on L.O.I.), and the compositions of these samples may have been slightly modified by late-stage alteration. Based on their TiO_2, Nb and LREE concentrations the volcanic rocks are subdivided into three groups: depleted, transitional and enriched basalts (Table 1). The classification is based on the elements, which are generally thought to be low-mobile and immobile during secondary alteration processes (for details see Discussion, Section 6.1 "Post-magmatic alteration"). All the samples are subalkaline to alkaline (trachy-) basalts and basaltic andesites in the total alkali-silica diagram (Fig. 4A), which is not reliable though because of greenstone alteration. The SiO_2 versus Nb/Y classification diagram is more suitable and shows two groups of basalts: subalkaline and alkaline (Fig. 4B). In respect to the element relationships in the Al_2O_3–TiO_2 + FeO^* – MgO system the majority of subalkaline samples are high-Fe-tholeiites (Jensen, 1976; Fig. 4C).

Analyses of 23 representative samples are illustrated in Figs. 5–7. The principal major-element characteristics of both groups are variable MgO (2–8.6 wt.%) and Fe_2O_3(tot) (8.3–16.9 wt.%), resulting in Mg# between 20 and 63 (Table 1). The depleted samples have lower TiO_2, Al_2O_3, P_2O_5 and higher SiO_2, MgO and CaO compared to the transitional and enriched varieties (Fig. 5A–D).

5.1.1. Depleted basalts

The depleted tholeiitic basalts (Fig. 4C) are characterized by a relatively large range of Mg# and Fe_2O_3 contents over a restricted range of SiO_2 and by near-flat REE patterns (Table 1; Figs. 5 and 6); SiO_2 spans 47.2–48.9 wt.%, Mg# = 50–63, Fe_2O_3 = 9.7–14.2 wt/%, and Ni = 28–139 ppm; Al_2O_3 varies between 13.7 and 15.7 wt.% suggesting little, if any, fractionation of clinopyroxene and plagioclase (Fig. 5B). Concentrations of TiO_2, Fe_2O_3, Nb and La increase as MgO decreases (Fig. 5A, D, F, and G). The TiO_2 concentrations vary between 1.3 and 1.9 wt.%, and P_2O_5 is in the range 0.13–0.19 wt.%. Both TiO_2 and $Fe_2O_{3(tot)}$ increase with decreasing MgO suggesting fractionation of olivine and pyroxene (Fig. 5A and D). In this suite of basalts, La/Sm_n ranges from 0.6 to 1.0, and Gd/Yb_n ranges from 1.0 to 1.3 (Table 1). The REE patterns are flat to moderately LREE depleted (Fig. 6A) and display no Eu anomalies. The samples have subchondritic and near-chondritic Ti/Zr ratios, whereas Zr/Y ratios are supra- and near-chondritic independently of their #Mg. The ratios of Al_2O_3/TiO_2 and Zr/Nb are consistently high, 8.9 and 35.0, compared to 5.8 and 6.2 in the transitional and enriched varieties, respectively (average values; Table 1). The trace-element spectra are characterized by zero to small negative Zr anomalies (Zr/Zr^* = 0.7–1.0), and coupled with weakly fractionated HREE they suggest a mantle source of the basalts in the spinel stability field (Fig. 7).

Thorium–Nb–LREE inter-element relationships are not complex. The Zasur'ya depleted basalts have zero to negative Nb anomalies (Nb/La_{pm} = 0.80–1.05) and negative Th anomalies (Th/La_{pm} = 0.40–0.84) with respect to La, that form negative trends

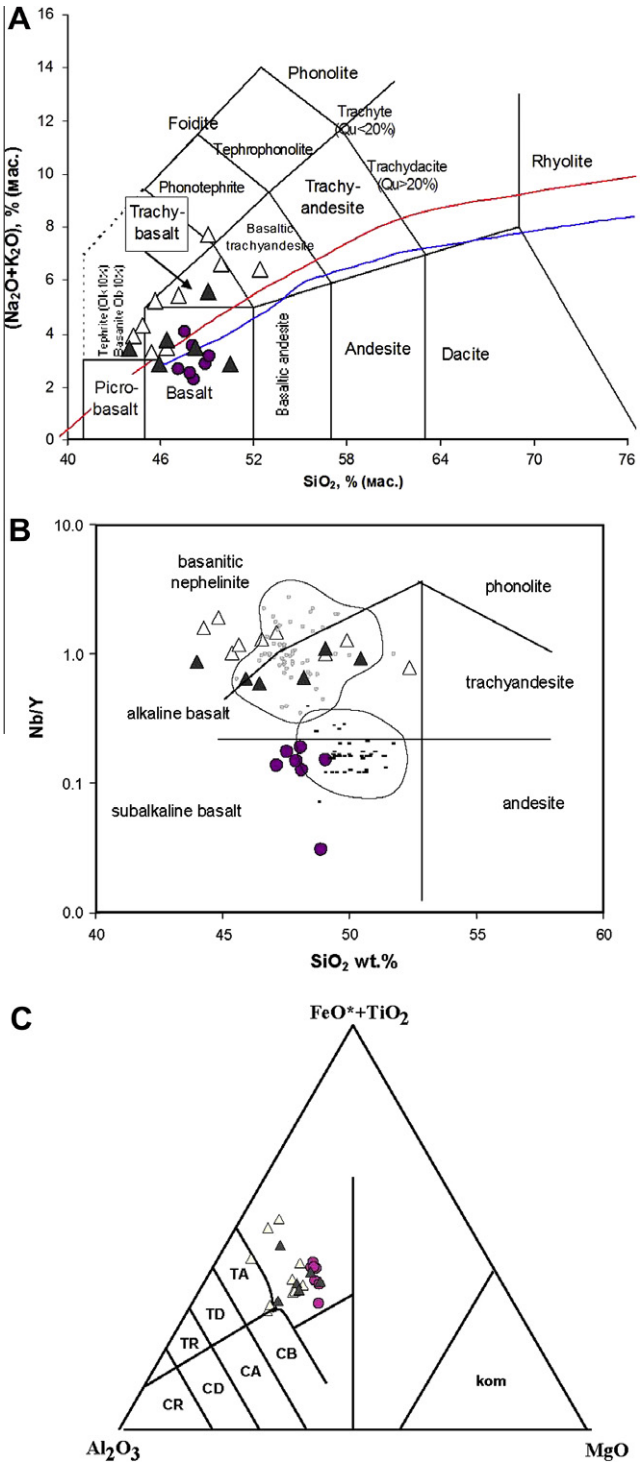

Fig. 4. Classification diagrams for Zasur'ya basalts (black circles – depleted basalts; triangles: black – transitional basalts, open – enriched basalts). A – TAS (Streckeisen et al., 2002). B – Nb/Y versus SiO_2 classification diagram (Winchester and Floyd, 1977). C – Al_2O_3–FeO^* + TiO_2 – MgO diagram (Jensen, 1976); tholeiitic series: TA – andesite, TD – dacite, TR – rhyolite; calc-alkaline series: CB – basalt, CA – andesite, CD – dacite, CR – rhyolite; kom – komatiite. Small dots (outlined): gray – Hawaiian hot-spot basalts; black – East Mariana Rise basalts, Western Pacific (GEOROC database (http://www.georoc.mpch-mainz.gwdg.de/georoc).

with La/Sm_n (Figs. 7, 8c), and positive Nb anomalies in respect to Th (Nb/Th_{pm} = 1.2–2.3; Fig. 7, Table 1). Thus, the samples plot as a cluster of negative Nb and Th anomalies over a range of La/Sm_n similar to those of Pacific MORBs (mid-oceanic ridge basalts) from the East Mariana Rise (Fig. 8A).

5.1.2. Transitional and enriched basalts

These basalts are defined on the basis of their positive Nb anomalies in the trace-element diagram (Fig. 7) and pronounced positively fractionated REE patterns, where La/Yb_n = 3.2–11 compared to La/Yb_n = 0.8–1.4 for the depleted counterparts (Fig. 6; Table 1). Relative to the suites of depleted tholeiitic basalts, they have higher contents of relatively or clearly incompatible elements (Ti, P, Th, La, Nb, Sm) at a given MgO value (Fig. 5A,C,E–H), greater incompatible/compatible element ratios, e.g., Zr/Y = 3.8–11.5 versus Zr/Y = 2.5–4.1, and moderately lower Zr/Nb = 3.4–9.0 and Al_2O_3/TiO_2 = 4.0–6.9 compared to Zr/Nb = 17–84 and Al_2O_3/TiO_2 = 7.3–10.4 (Table 1). Two types are present on the basis of major and trace element compositions: (1) transitional basalts; (2) enriched basalts. Both varieties occur as sheeted fragments within folded structures and it is impossible to identify their original geological relationships. Transitional basalts have generally higher MgO (6.9 vs. 5.3 wt.%), lower TiO_2 (2.6 vs. 2.9 wt.%), Al_2O_3 (15.3 vs. 16.8 wt.%) and most trace element contents, and less fractionated REE (La/Yb_n = 4.0 vs. 6.7 av.) than the enriched counterparts (Table 1; Fig. 5A, B, and F). Both types of basalts show LREE enrichment though to a different degree (Fig. 6). Transitional and enriched basalts show less Th depletion over La (Th/La_n = 0.8 vs. 0.9) compared to depleted basalts (Th/La_n = 0.6). Both transitional and enriched varieties are characterized by clear positive anomalies of Nb with respect to La: Nb/La_{pm} = 1.6 and 1.4 (averages), respectively (Table 1, Fig. 7). A subset of the enriched varieties have pronounced negative Zr anomalies (Zr/Zr^* = 0.43–0.7), which together with fractionated HREE suggest their mantle source was within the garnet stability field (Table 1; Figs. 6 and 7). Similar trace element patterns have been documented for many Phanerozoic transitional to enriched OIB-type basalts hosted by accretionary complexes of Central Asia, Far East and Japan (e.g., Chen et al., 1991; Ichiyama et al., 2008; Safonova, 2008, 2009; Safonova et al., 2009), and Proterozoic and Archean volcanic rocks interpreted as ocean island basalts (e.g., Stern et al., 1995; Polat et al., 1999; Komiya et al., 2004).

In the diagrams of highly incompatible elements, such as Nb versus Th, Nb versus La/Yb and Nb versus Y (Fig. 9A and B), the depleted basalts plot near the modern MORB and the oldest seamounts of the Emperor-Hawaii Chain of Seamounts (EHCS; Regelous et al., 2003) – Detroit and Meiji (81–84 Ma). The transitional basalts plot near the points of younger seamounts of the EHCS – Nintoku and Koko (43–56 Ma). The compositional points of the enriched basalts are close to those of the Hawaii Islands (0–2 Ma). In the Nb versus Y diagram (Fig. 9C) the three groups of basalts plot along three different trends due to variable Y/Nb ratio: 7.6 for the depleted group, 1.3 – for transitional and 0.8 – for enriched varieties (average values; Table 1).

5.2. Sr–Nd isotopic compositions

The paper presents first Sr and Nd isotopic data for Zasur'ya oceanic basalts, two depleted (Zas-21-07, Zas-22-07), two transitional (G2921, E2921) and two enriched (Zas-23-07, Zas-30-07) samples, which were corrected for radioactive decay since eruption. The initial isotopic ratios were corrected to 500 Ma – a conventional average of the Late Cambrian–Early Ordovician age range of Zasur'ya basalts. The ε_{Sr} and ε_{Nd} values are reported relative to CHUR. The enriched samples have the initial $^{87}Sr/^{86}Sr$ ratios of 0.70571, 0.70633 and 0.70231 and $\varepsilon_{Nd}(t)$ values of 7.0, 7.1 and 6.6, respectively (Table 2; Fig. 10). The transitional samples have the initial $^{87}Sr/^{86}Sr$ ratios of 0.70473 and 0.70547, and $\varepsilon_{Nd}(t)$ values of 6.3 and 8.5, respectively. The depleted samples have the initial $^{87}Sr/^{86}Sr$ ratios of 0.70467 and 0.70430, and $\varepsilon_{Nd}(t)$ values of 8.4 and 9.9. The relatively stable Nd and the more variable Sr data (possibly affected by alteration; see below), may reflect derivation

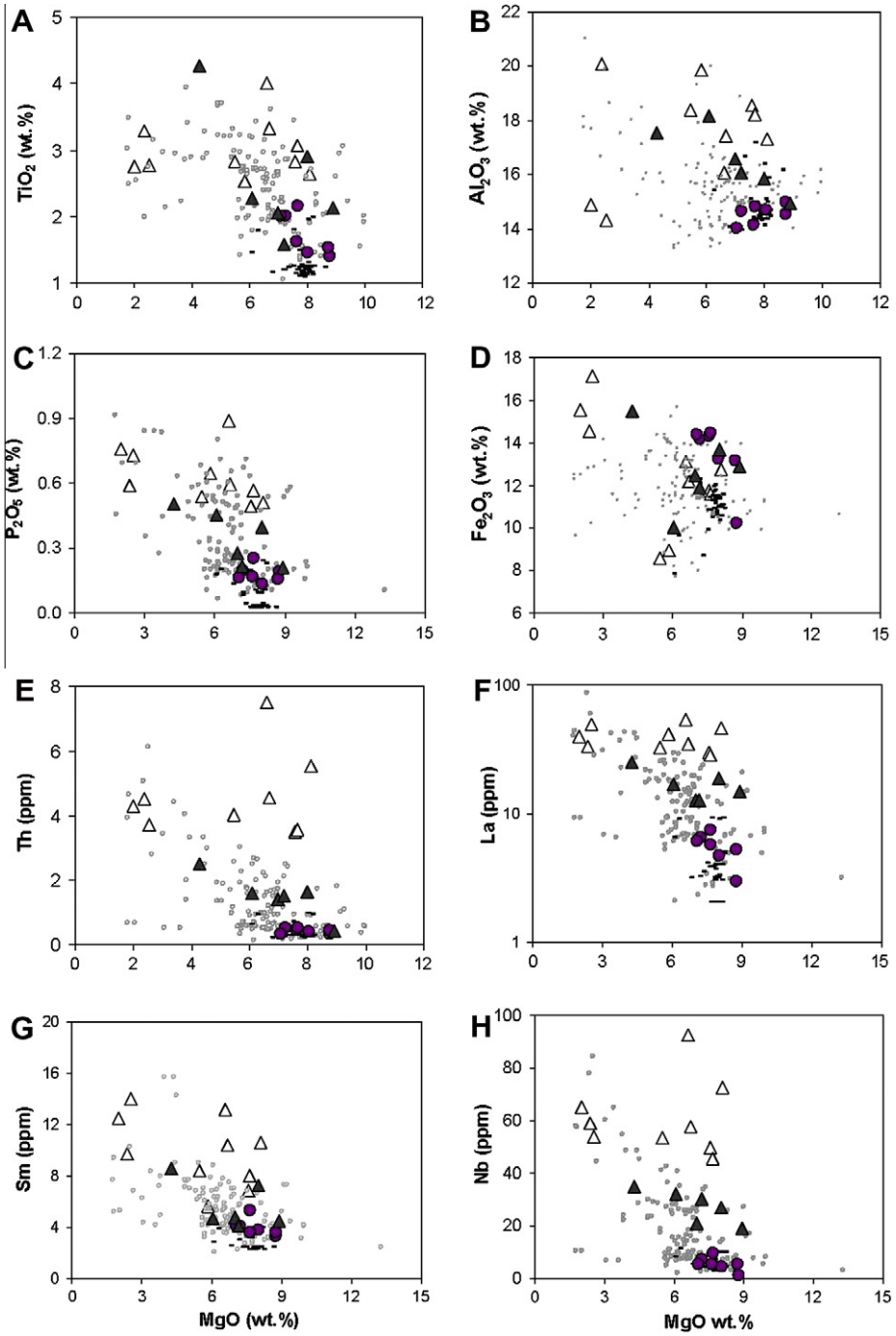

Fig. 5. Major and trace element data versus MgO (wt.%) for oceanic basalts from the Zasur'ya accretionary complex. Symbols as in Fig. 4.

from different types of mantle or from a heterogeneous mantle source, that is typical of plume-related intra-plate basalts (Safonova, 2008), or a different/complex magma generation process, and alteration superimposed on all this. A similar situation was mentioned for Permian plume-related mafic dykes of the Emeishan LIP (Zi et al., 2008). In the $(^{87}Sr/^{86}Sr)_i$ versus $\varepsilon_{Nd}(t)$ diagram, the samples plot near the field of HIMU (OIB) and DM (MORB) (Fig. 10).

Generally, the range of initial $^{87}Sr/^{86}Sr$ values is much wider than those for oceanic tholeiites, reported from the modern MORB and OIB. Most samples plot in the "prohibited" right-upper quadrant in Fig. 10. Mahoney et al. (1998) observed a similar result for leached, old, highly altered basalts, and attributed this to incorporation of non-magmatic Sr into the crystal structure during replacement of plagioclase by secondary feldspar. Therefore, we interpret this as a result of post-magmatic alteration of sea-floor conditions. If we boldly project the plotted point to the vertical axes we will find them within the HIMU/OIB field. The Sr and Nd isotopic compositions of similar rocks from the Altai-Sayan folded area (Yarmolyuk and Kovalenko, 2003; Utsunomiya et al., 2009) as well as from the Aruba oceanic plateau (White et al., 1999) also fall within the right-upper-quadrant range of our samples. Thus, if ignoring the post-magmatic alteration processes, the value of the Zasur'ya enriched samples overlap with the field defined by OIB-type lavas in terms of their Sr–Nd isotopic compositions. The depleted samples have initial $^{87}Sr/^{86}Sr$ ratios higher and ε_{Nd} slightly lower than typical MORB (Fig. 10). There is no direct correlation

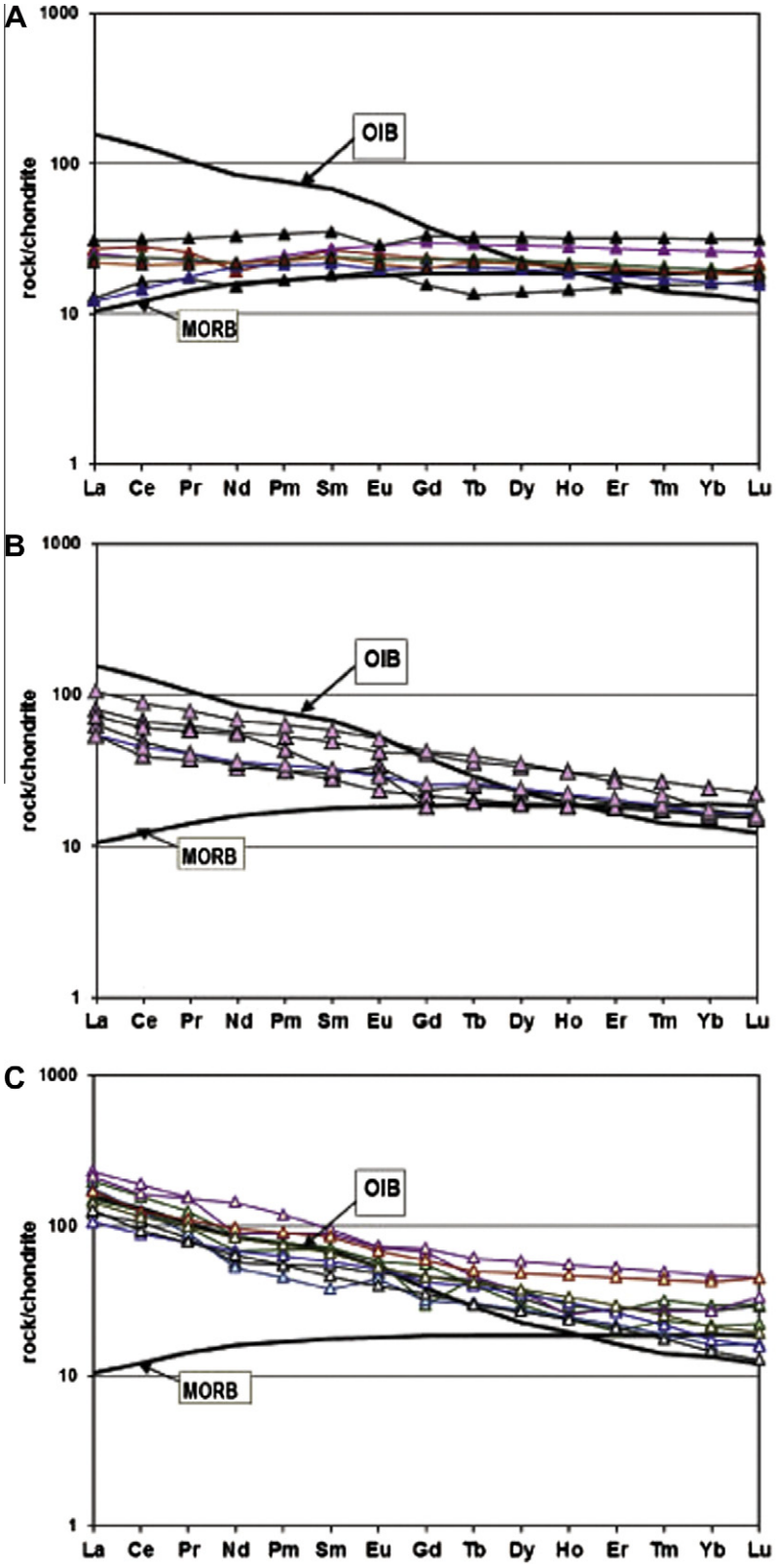

Fig. 6. Chondrite-normalized rare-earth element patterns for the Zasur'ya depleted (A), transitional (B) and enriched (c) lavas. OIB, MORB and normalization values are from Sun and McDonough (1989). Symbols as in Fig. 4.

between isotope ratios ($^{143}Nd/^{144}Nd$ and $^{87}Sr/^{86}Sr$) and the degree of LREE enrichment in the plume-type transitional and enriched samples; hence, it can be supposed that the source of the enriched basalts was enriched shortly before the derivation of basaltic melt or they were derived from different mantle sources.

6. Discussion

In order to discuss the origin of three basaltic units, we must evaluate possible effects of secondary post-magmatic alteration, crustal contamination and fractional crystallization on their com-

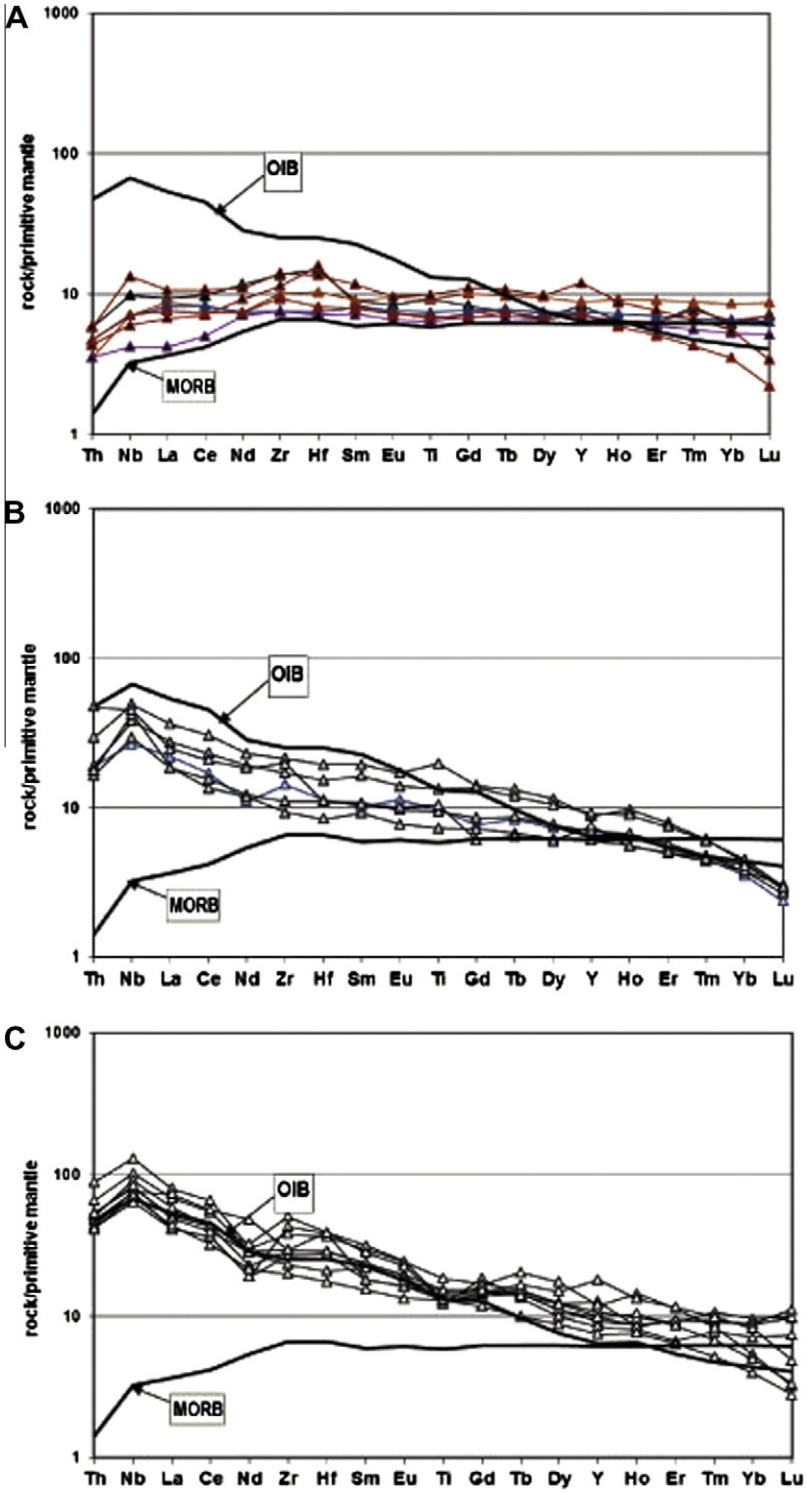

Fig. 7. Primitive mantle-normalized multi-component trace-element diagrams for the Zasur'ya depleted (A), transitional (B) and enriched (C) lavas. OIB, MORB and normalization values are from Sun and McDonough (1989). Symbols as in Fig. 4.

position in general and the concentrations of highly incompatibles elements, e.g., Th, Nb and LREE, specifically, because we regard the key elements in differentiating oceanic (OIB, OPB, MORB) and continental margin (island/back/fore-arc) basalts.

6.1. Post-magmatic alteration

Variable element mobility is a possibility for Paleozoic volcanic rocks that have undergone sea-floor hydrothermal alteration and greenschist to epidote–amphibolite facies metamorphism induced by polyphase accretion and subsequent collision, but there is a general agreement that the most of the REE, HFSE and some transitional metals are least sensitive to mobility (Winchester and Floyd, 1977; Rollinson, 1993 and references cited therein). Light REE are more sensitive to secondary processes compared to middle and heavy REE, however the mobility of REE takes place only at high water/rock ratio or during carbonatization (Humphris, 1984), which is not observed in our case. Those samples with the

values of L.O.I. exceeding 4 wt.% or large Eu anomalies were not used for petrogenetic interpretation. Primary clinopyroxene is sporadically present in the Zasur'ya basalts. However, intense structural transposition which resulted in abrupt lithological changes in many of the Zasur'ya sedimentary and volcanic rocks inhibits detailed individual flow scale alteration study.

In the studied set of least altered basaltic rocks, evidence for low mobility of HFSE, REE (except Eu) and, to a lesser degree, Th includes the following: (1) there is no significant enrichment or depletion of groups of elements (e.g., light REE) in a given rock type over a range of L.O.I. (Fig. 6; Table 1); (2) primitive mantle-normalized trace-element diagrams of given suites of basalts associated in the field exhibit coherent patterns for Th, HFSE, and REE (Fig. 7); (3) Th–Nb–La inter-element relationships do not correlate with the CIA (chemical index of alteration; not shown here), Eu/Eu*, or loss on ignition (Fig. 11A–C; Safonova, 2005). So, all these features also perhaps emphasize the excellent inter-element correlations between Th, Nb and La.

Similar conclusions concerning the relative immobility of Ti, REE and HFSE in ancient volcanic rocks that have experienced alteration under conditions of low water–rock ratios have been reached by workers in Phanerozoic accretionary complexes of Central Asia including Altai-Sayan (e.g., Simonov et al., 1994; Safonova, 2005; Safonova et al., 2009; Utsunomiya et al., 2009), and in older Archean terranes (e.g., Polat et al., 1999; Jochum et al., 1991; Komiya et al., 2004). Thus, emphasis is placed on HFSE, REE and Th that are relatively immobile during secondary processes.

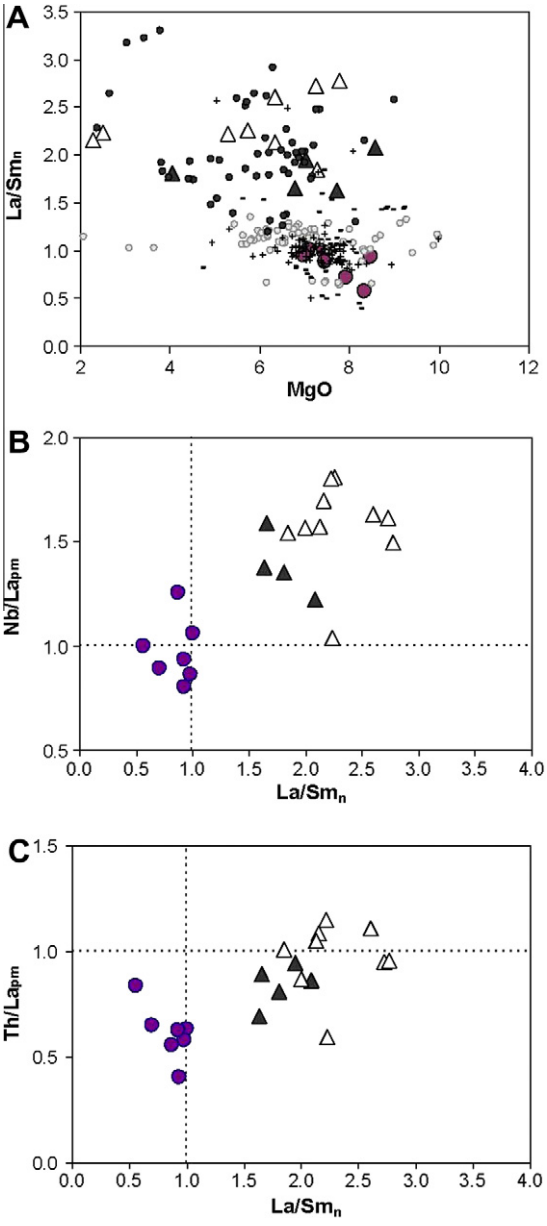

Fig. 8. La/Sm$_n$ versus MgO, Nb/La$_{pm}$ and Th/La$_{pm}$ for the three basaltic suites indicating that crustal contamination did not influence the Th–Nb–La systematics. Symbols as in Fig. 4.

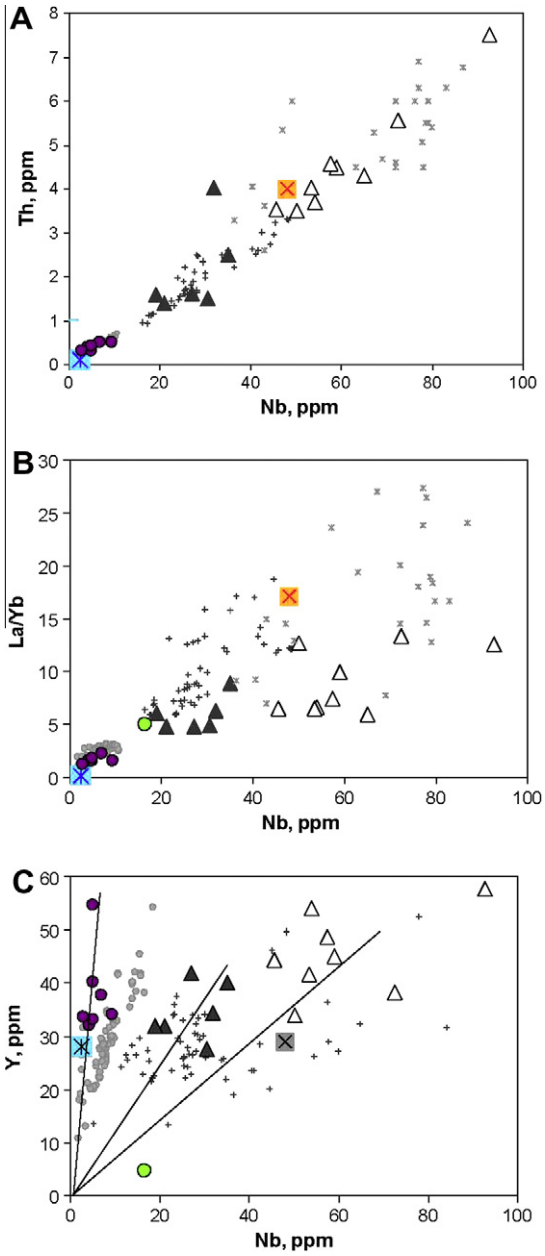

Fig. 9. Nb versus Th (A), La/Yb (B) and Nb versus Y (C) variations in the Zasur'ya lavas. Data for Emperor Seamount tholeiites (older – gray circles, younger – crosses; Regelous et al., 2003), Hawaii (GEOROC database – small stars), and average values of bulk crust (green circle), N-MORB (star in square; Sun and McDonough, 1989) and OIB (X-cross in square; Sun and McDonough, 1989) are shown for comparison. Other symbols see in Fig. 4. (For interpretation of the references to colour in this figure legend, the reader is referred to the web version of this article.)

Table 2
Sm–Nd and Rb–Sr isotope data for Zasur'ya basalts.

Sample	1 Rb*	2 Sr*	3 $^{87}Rb/^{86}Sr$	4 $^{87}Sr/^{86}Sr$	5 $2\sigma_m$	6 $I_{Sr}(500)$	7 Sm*	8 Nd*	9 $^{147}Sm/^{144}Nd$	10 $^{143}Nd/^{144}Nd$	11 $2\sigma_m$	12 ε_{Nd}	13 $2\sigma_m$	14 $\varepsilon_{Nd}(500)$
Zas 21-07	4.70	211.2	0.0644	0.705130	13	0.70467	4.17	13.6	0.18571	0.513031	13	7.7	0.26	8.4
Zas 22-07	9.21	231.4	0.1152	0.705117	15	0.70430	2.96	8.81	0.20335	0.513165	8	10.3	0.16	9.9
G 2921	2.91	177.3	0.0475	0.705064	12	0.70473	3.23	10.5	0.18667	0.512930	6	5.7	0.12	6.3
E 2921	17.4	415.7	0.1213	0.706338	7	0.70547	4.21	16.7	0.15276	0.512928	4	5.6	0.09	8.5
Zas 23-07	11.5	336.0	0.0993	0.706422	7	0.70571	6.45	28.2	0.13843	0.512806	9	3.3	0.17	7.0
Zas 30-07	8.16	700.3	0.0337	0.706571	7	0.70633	6.76	32.4	0.12609	0.512771	6	2.6	0.11	7.1

* Concentrations in ppm.

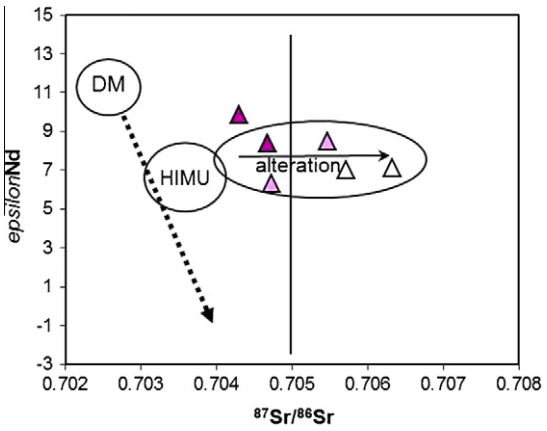

Fig. 10. Initial $^{87}Sr/^{86}Sr$ versus ε_{Nd} values of the Zasur'ya lavas. DM and HIMU fields are from Zindler and Hart (1986).

6.2. Crustal contamination

Contamination by continental crust is a possibility for mafic magmas; however, several lines of geological evidence are consistent with an intra-oceanic setting for the basalt sequences (Sections 1 and 2). The presence of multi-colored sandstones and cherts with oceanic radiolarian and conodonts interlayered with pillowed basalts and flows suggests an oceanic environment for the eruption of the volcanic rocks (Buslov et al., 1999, 2000, 2001; Sennikov et al., 2003; Safonova et al., 2004).

Generally speaking, most crust contaminated mafic lavas are characterized by high Th contents and Nb negative anomalies relative to Th and La in trace-element diagrams. The Zasur'ya depleted, transitional and enriched lavas display no negative Nb anomalies in respect to Th (Figs. 8 and 9). Several depleted samples possess weak Nb depletion relative La (Nb/La_{pm} = 0.8–0.9; Fig. 8B). However, SiO_2, MgO, Ni, Cr and LREE contents in these basalts do not correlate with the magnitude of negative Nb anomalies as is expected for crustal contamination (Table 1). Those trends are present in crustally contaminated basalts of Western Australia and Early Proterozoic basalts of the Baltic shield (Redman and Keays, 1985; Arndt and Jenner, 1986; Putchel et al., 1997; Polat et al., 1999). Additionally, the presence of profound positive Nb anomalies, low Al_2O_3/TiO_2 and Th/La_{pm} ratios in most of the spatially associated transitional and enriched basalts, rules out contamination of these basalts by continental crust (Fig. 9; Table 1). Besides, the high concentrations of LREE in some transitional and in most enriched basalts preclude any significant crustal contamination since average continental crust is characterized by much lower LREE and distinctly different REE patterns (Taylor and McLennan, 1985). This conclusions is also supported by high concentrations of other incompatible elements such as Zr (~350 ppm), Nb (~60 ppm), Ti (~2.9 wt.%), and Th (~4 ppm) in those basalts.

The noted above geochemical features taken with geological evidence for an intra-oceanic setting in these suites, suggest that the low Nb/La_{pm} values found in some of the Zasur'ya tholeiites may reflect a subduction-derived component in the mantle rather than crustal contamination. However, subduction-related lavas are usually characterized by positive Th anomalies relative to La ($Th/La_{pm} > 2$; Safonova et al., 2009), that is not observed in our case. The low Nb/La_{pm} values in those depleted samples does not result from contamination of tholeiitic liquids by continental crust during magma upwelling and eruption (exogeneous contamination), but may have resulted from recycling of lithosphere into the mantle (endogeneous contamination with mafic oceanic crust material; Fig. 8; Polat et al., 1999). Thus, geological relationships with OPS sediments and their lithology and geochemical and isotopic features of the Zasur'ya basalts are inconsistent with basalt magma contaminated by continental crust.

6.3. Fractional crystallization

The range of Mg# in most samples of basalts is not wide enough (Fig. 5) to test fractional crystallization control on Nb anomalies. Nb is not compatible in clinopyroxene, but in Fe–Ti oxides which can be fractionating phases in mafic liquids. However they are stable under high oxygen fugacities, which are more typical of subduction-related magmas. Fowler and Jensen (1989) modeled the evolution of Mg- to Fe-tholeiites in the Kinojevis group of the Abitibi belt: they found that the compositional range could be accounted for by fractional crystallization of olivine, clinopyroxene, plagioclase, and Fe–Ti oxides. The limited variation of La/Sm_n ratios over a wide range of MgO contents within each group of basalts (Fig. 8A) suggests that there was no significant LREE fractionation as a result of fractional crystallization of clinopyroxene, and there is no correlation of Nb anomalies with Mg# (Fig. 11D). Fe–Ti oxides may accommodate Nb, but there is no clear correlation of Nb/La_{pm} with Ti/Ti^* (Fig. 11E) and Fe_2O_3 contents in the Zasur'ya basalts. Consequently, Th–Nb–LREE inter-element ratios in the transitional and enriched lavas are independent of olivine, clinopyroxene, plagioclase or Fe–Ti oxide fractionation or accumulation, however, such a tendency is not obvious in the depleted basalts (Fig. 11D–F) suggesting their different origin.

6.4. Mantle sources and melting

If we accept that post-eruption alteration, fractional crystallization and crustal contamination did not affect the Th–Nb–LREE systematics, then the variations of these elements in the transitional and enriched basalts may be a signature of compositionally heterogeneous mantle, as is observed in Phanerozoic and Cenozoic oceanic plateaus such as Ontong Java (Polat et al., 1999; Mahoney et al., 1993; Neal et al., 1997) and the oceanic islands of Iceland and Hawaii (e.g., Hards et al., 1995; Regelous et al., 2003). As far as Nb, La and Th have similar partition coefficients, they are unlikely to be fractionated from one another during the relatively high

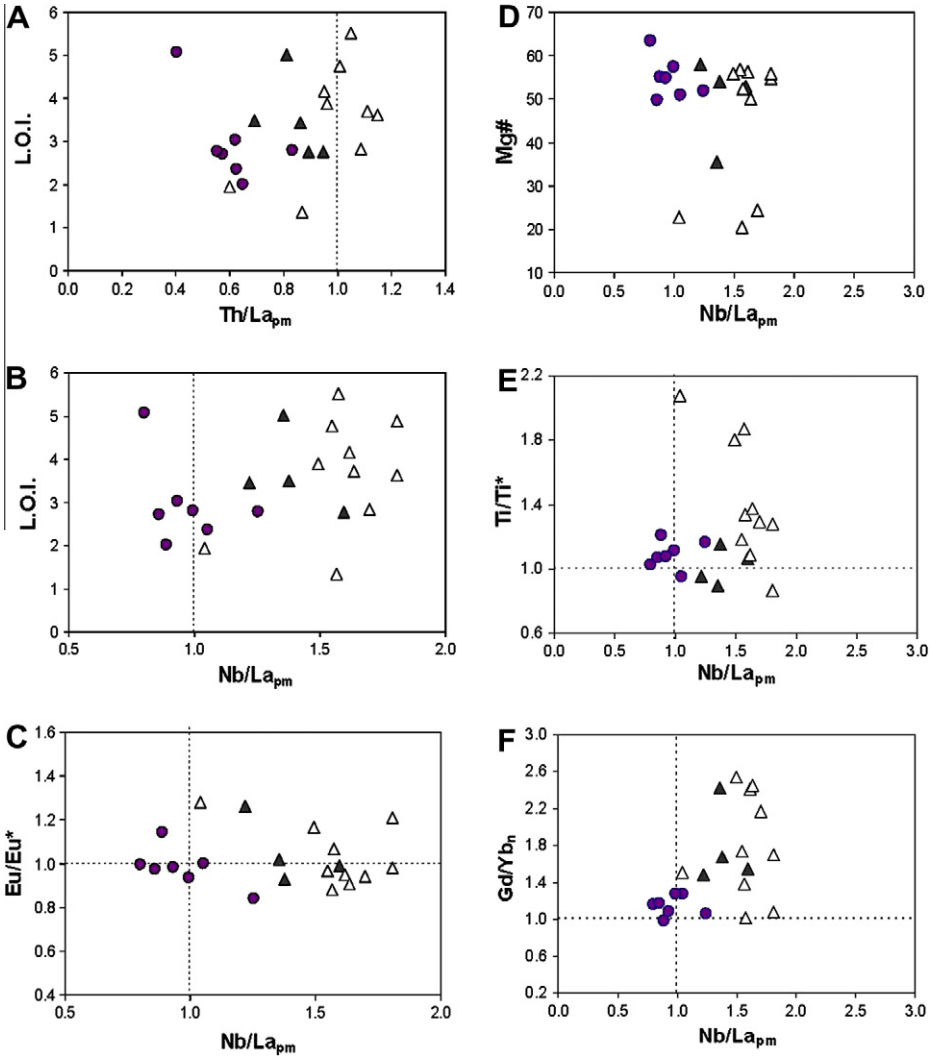

Fig. 11. Binary ratios for the Zasur'ya three basaltic suites, indicating that Th–Nb–La inter-element ratios weakly correlate with alteration and metamorphism (A and B) and with fractional crystallization (D–F). The dashed lines are primitive mantle ratios (from Sun and McDonough, 1989). Symbols as in Fig. 4.

degrees of partial melting involved in the genesis of mafic oceanic lavas (Polat et al., 1999 and the references cited therein).

The medium to high differentiation of HREE (Gd–Yb$_n$ = 1.5–2.4) in the most of Zasur'ya transitional and enriched samples may reflect mantle melting in the garnet stability field (e.g., Green, 1994; Hirschman and Stolper, 1996; Fig. 6B and C), because garnet preferentially sequesters the HREE into its structure. Besides, the higher enrichment of the transitional and enriched varieties in Nb compared to the depleted group is typical of plume-related volcanic rocks, i.e., OIBs (e.g., Sun and McDonough, 1989; Figs. 5G, 7, 9). Saunders et al. (1988) supposed that Nb resides in the subducting oceanic slab, whereas LREE and Th are fractionated from it to be transferred to the subarc mantle. Nb is an element compatible in Fe–Ti oxides only, such as rutile, which dominates the budget of incompatible elements relative to LREE in the eclogites formed during subduction (Rudnick et al., 2000). Nb can fractionate from Th and LREE through subduction-induced dehydration and accumulate through the mixing of subducted oceanic slabs back into the lower mantle, possibly reaching the core–mantle boundary (McCulloch and Gamble, 1991; Brenan et al., 1994). The medium to high HREE fractionation of most enriched basalts coupled with positive to negative Zr anomalies suggest spinel to garnet facies depths of melt segregation in the mantle, i.e., below and above

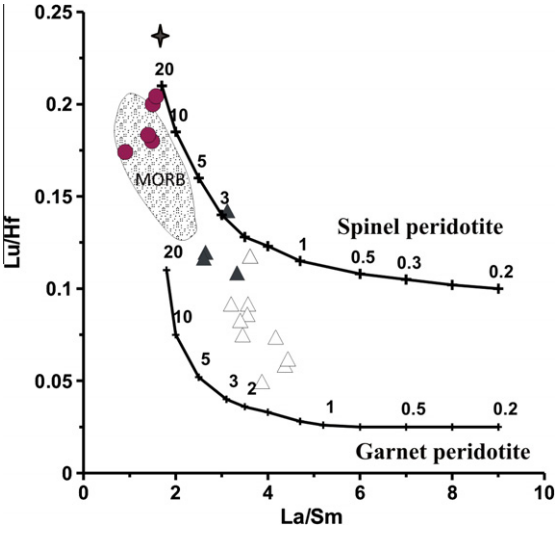

Fig. 12. Lu/Hf versus La/Sm in the Zasur'ya lavas. The curves are taken from (Regelous et al., 2003) and show the effect of the equilibrium melting of spinel and garnet peridotites between 0.01% and 20%. The source (star) has primitive mantle composition (Sun and McDonough, 1989). The transitional and most of enriched lavas are mixtures of spinel and garnet peridotite melts formed at low to medium degrees of melting. The depleted lavas have low La/Sm and high Lu/Hf ratios which are indicative of even higher degrees of melting within the spinel stability field.

the 400 km level, whereas the depleted basalts melted at even shallower depths in the entrained upper mantle.

In the La/Sm versus Lu/Hf diagram (Fig. 12) showing the melting curves for spinel and garnet peridotite the Zasury'a depleted tholeiites clearly plot within the MORB field, whereas the transitional and enriched varieties are likely to be mixtures of melts of both spinel and garnet peridotite. The low La/Sm and high Lu/Hf ratios of the depleted basalts require relatively large degrees of melting within the spinel stability field, of a source with lower La/Sm than primitive mantle. Alternatively, the enriched basalts likely formed at lower degrees of partial melting in both spinel and garnet stability fields.

Thus, the mantle plume column may be heterogeneous and contain mixed enriched and depleted melts resulting in variable enrichment in incompatible elements, such as Ti, REE, Nb and Th (e.g., Silver et al., 1988; Mahoney et al., 1993; Hards et al., 1995). The degree of such enrichment probably depends on the degree of partial melting (Regelous et al., 2003 and references therein; Table 1; Figs. 6, 12 and 13). Younger seamounts formed over thin oceanic lithosphere and/or close to mid-oceanic ridge spreading zones (Regelous et al., 2003; Safonova, 2008) may have lower concentrations of Nb and less profound Nb anomalies compared to typical OIB (Figs. 9, 11B,C). Those basalts, like the older seamounts of the Emperor Seamount Chain (Meiji, Detroit), possess flat REE patterns, which are indicative of shallower depth and/or higher degrees of melting (e.g., Hofmann, 1997; Polat et al., 1999; Regelous et al., 2003; Figs. 7 and 12). Near-flat HREE patterns of some Zasur'ya transitional and enriched basalts are furthermore consistent with a shallower melting depth (Safonova, 2008).

A part of depleted have Nb and Th negative anomalies (Figs. 7A, 11B,C; Table 1) that also can be attributed to compositionally heterogeneous mantle plumes, incorporating a recycled subduction-derived component ($Nb/La_{pm} < 1$) and a residual slab derived component ($Nb/La_{pm} > 1$) into the mantle (Polat et al., 1999 and the referenced cited therein). There is no evidence for recycled sediments because there are no samples with negative Nb but positive Th anomalies.

Many investigators have shown that the Cretaceous to Quaternary plume-related oceanic plateau and island basalts, e.g., Ontong Java, Hawaii, Iceland, etc., have diverse geochemical compositions and several mantle components (Neal et al., 1997; Wilson, 1993; Hemond et al., 1993). Like the Zasur'ya basalts, other western Altai-Sayan folded structures also have tholeiitic basalts with a wide range of trace element (Th, HFSE, REE) characteristics suggesting that Late Neoproterozoic–Early Paleozoic mantle plumes in general may also have contained several mantle source components (Safonova, 2008; Safonova et al., 2009). These different components, partly derived from lithosphere recycling, have not formerly been identified in the Early Paleozoic mantle based on trace element systematics.

6.5. Tectonic Implications

6.5.1. Tholeiitic basalts

The Zasur'ya tholeiites are characterized by medium TiO_2, weakly LREE depleted to flat REE patterns, zero to slightly negative Nb anomalies relative La and positive Nb anomalies relative to Th (Table 1; Figs. 6A, 7, 9). These geochemical features have been found in basaltic lavas formed in mid-oceanic ridge or oceanic plateau or even oceanic island setting. Oceanic plateau basalts (OPB) have been compared with those of oceanic islands (OIB) by many investigators (e.g., Floyd, 1989; Mahoney et al., 1993; Neal et al., 1997). Ocean plateaus (OPBs) comprise extensive and structurally and compositionally uniform tholeiites and are the oceanic counterparts of continental flood basalts. In contrast, ocean islands have topographically pronounced volcanic buildings, and generally include tholeiitic, transitional and alkaline basalts. Mid-oceanic ridge basalts compose the ocean floor and often occur at the base of oce-

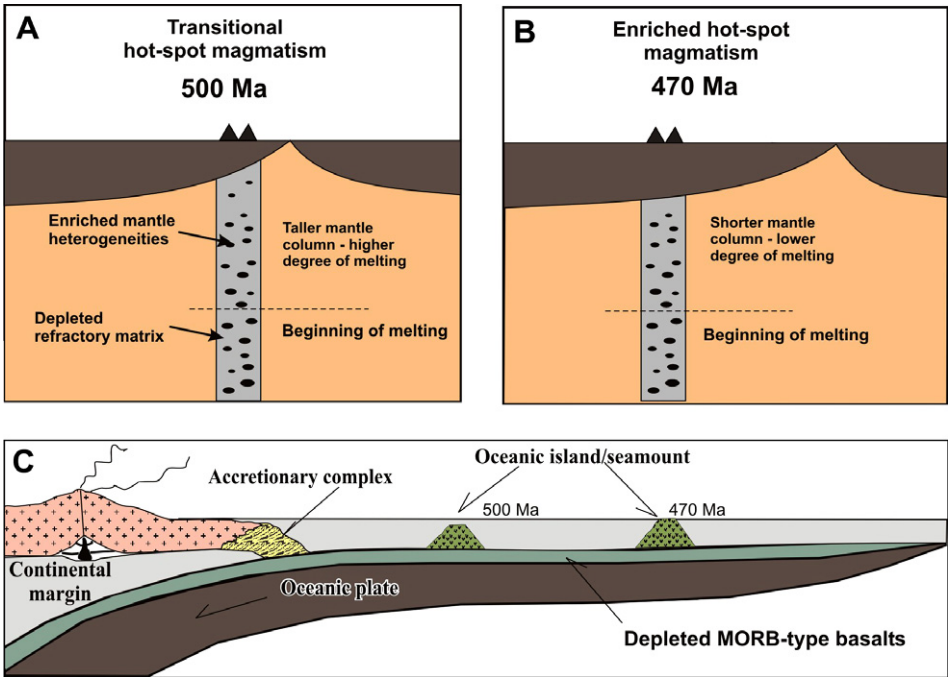

Fig. 13. Scheme for the 500 Ma transitional (A) and 470 Ma enriched (B) hot-spot oceanic basalts (Groups 2 and 3) of the Zasur'ya AC (adapted from Regelous et al., 2003; for age implications see Section 6.5.2) in respect to the thickness of the oceanic lithosphere. At 500 Ma the lavas probably erupted closer to MOR, i.e., under a thinner/younger oceanic lithosphere. This resulted in the relatively high degrees of melting and therefore in a larger portion of incompatible element depleted refractory material in the melt. At 470 Ma, when the plume is located under a thicker but older oceanic lithosphere, the melting column was shorter, the average degree of melting was lower and the melt was more contributed by incompatible element enriched less refractory material of mantle heterogeneities. C – in the Ordovician the crust of the PAO subducted beneath the SW active margin of the Siberian continent.

anic rises. Although, unlike MORB, many OPBs have "transitional" chemistries with inter-incompatible element ratios similar to chondrite or bulk silicate Earth we decline the plateau setting of formation for the Zasur'ya depleted basalts because, like it was mentioned, the size of most presently known oceanic plateaux is very big. Therefore, it is unlikely that even strong tectonic events like strike-slip faulting could completely destroy such a giant structure. In the Zasur'ya AC we observed only small fragments of basaltic units – up to several meters thick and tens meters long. However, the fragments of most accreted oceanic plateaus, ranging in age from the Archean to the Cretaceous, are large slivers up to hundreds meters thick and many kilometers long (Kerr et al., 2000 and the references cited therein).

We also decline a plume-related origin of the depleted melts because in the most incompatible element diagrams they are plotted separately from the transitional and enriched varieties, which hot-spot origin will be discussed below. Moreover, in the Nb versus Y diagram (Fig. 9C) the depleted basalts plot along a separate line, which lies notably steeper than the trend of the most depleted basalts in the EHCS, i.e., those of the oldest Meiji and Detroit Seamounts (Figs. 8A, 9A,B). Finally, the depleted unit occurs structurally below the units hosting transitional and enriched basalts. Thus, based on both geological and geochemical data we conclude that the Zasur'ya depleted basalts having flat REE patterns and the most pronounced Nb depletion relative La may be analogs of Phanerozoic mid-oceanic ridge basalts, that is supported by Nb versus Y and La/Sm versus Lu/Hf diagrams (Figs. 9C, 12). They probably represent a base of the Zasur'ya oceanic island/seamount consisting of transitional and enriched basalts.

6.5.2. Transitional to alkaline basalts

Basalts of transitional to enriched incompatible element composition with strongly fractionated REE and high Nb contents are rather abundant in the Zasur'ya Series of the Charysh-Terekta strike-slip zone (Sennikov et al., 2003; Safonova et al., 2004, 2009). The transitional basalts are similar to Fe-tholeiites; they have pronounced REE fractionation and zero to positive Zr anomalies. The weak HREE fractionation coupled with zero Zr and Hf anomalies in a part of enriched samples signify that their paternal basaltic liquids segregated in the spinel-facies deep mantle (Fig. 9C). Transitional and enriched basalts have Zr/Hf and Nb/Ta ratios that extend to slightly higher average values than the respective mantle values of 36 and 16 in common with many Phanerozoic and Cenozoic within-plate basalts (Kamber and Collerson, 2000; Green et al., 1989, Table 1).

It is quite possible that the Zasur'ya transitional basalts were related to hot-spot volcanism, but erupted over a thinner oceanic lithosphere and/or closer to mid-oceanic ridge than the enriched basalts (Fig. 13A and B). Such a tendency was noted before between the older (Detroit and Meiji; 81–83 Ma) and younger (Nintoku, Daikakuji; 55–42 Ma) seamounts of the EHCS in the Pacific Ocean (Regelous et al., 2003) and between the older Kurai (600 Ma) and younger Katun (540 Ma) Paleoseamounts of the PAO (Safonova, 2008). However, taking into account the average velocity of oceanic subduction and the growth of the oceanic lithosphere thickness (e.g., Parsons and Sclater, 1977; Reid and Jackson, 1981) the age difference between more depleted (transitional in our case) and enriched basalts erupted over one hot-spot and one oceanic plate, like in the EHCS, must be at least 30 Ma, i.e., approximately equal to the time interval between the Late Cambrian and Early Ordovician, which was estimated by micropaleontological data (Sennikov et al., 2003, 2004). Therefore, for our interpretations we suggest that the older seamount could ne early Late Cambrian with an average age of 500 Ma and the younger seamount could ne Latest Cambrian to Early Ordovician with an average age of 470 Ma.

6.6. Geodynamic model

Contacts between the oceanic island/seamount and ridge units are likely tectonic in the Charysh-Terekta strike-slip zone (Buslov et al., 2000, 2004b). The tectonic strike-slipping destroyed original geological relationships and the tectonic interleaving has not previously been addressed in detail, in part because of the difficulty in distinguishing various basalt subtypes in outcrop. Previously it was shown that the structural and field relations of imbricated lithotectonic units in the Charysh-Terekta strike-slip zone (Buslov et al., 2001) are comparable with modern accretionary complexes, e.g., Naizawa accretionary complex of the Idonappu zone in Hokkaido, Japan (Ueda et al., 2000), over a wide range of scales. The presented geochemical results support this idea and suggest that the mid-oceanic ridge tholeiitic sequences relatively depleted in Nb may be tectonically juxtaposed with accreted ocean island/seamount basaltic sequences possessing positive Nb anomalies relative La and Th (Fig. 7).

Structural complexity of the Charysh-Terekta strike-slip zone in particular, and in Late Neoproterozoic–Early Paleozoic accretionary belts in the western Altai-Sayan in general, creates a major difficulty in identifying all these tectonic entities (Buslov et al., 2000, 2001; Safonova et al., 2004). The spectrum of positive to negative Nb anomalies, and Th/La_{pm} ratios mainly <1 in the Zasur'ya basalts, flat REE patterns of MORB-type tholeiites and the presence of LREE-enriched OIB-type alkaline basalts are compatible with the accretionary complex model of Buslov et al. (2000). A similar structure of the accretionary wedge was deduced for younger accretionary complexes in the Western Pacific, Japan (Wakita, 2000; Isozaki et al., 2010). Another evidence for the oceanic island environment for the alkaline basalts comes from their spatial association with seamount slope-type radiolarian cherts and other siliceous beds (Sennikov et al., 2003, 2004).

Based on the detailed analysis of geochemical data, previously reported geological and lithological data (Sennikov et al., 2003, 2004) and tectonic implications (Buslov et al., 1999, 2000) we propose the following tectonic model for the formation of the oceanic basalts of the Zasur'ya accretionary complex (Fig. 13). In Late Cambrian time, a spreading zone was located in the Ob'-Zaysan branch of the PAO and produced mid-oceanic ridge basalts, the Zasur'ya depleted basalts, which became a part of the oceanic floor. At that time the mantle plume located beneath the PAO oceanic lithosphere induced hot-spot volcanism, which produced seamounts/islands. The seamounts built in the early Late Cambrian, i.e., over a younger/thinner oceanic lithosphere, consisted of relatively enriched incompatible element basalts – the Zasur'ya transitional basalts (Fig. 13A). The seamounts formed later, i.e., in the latest Late Cambrian Ordovician, which lavas erupted on the older/thicker oceanic crust, were composed of stronger incompatible element enriched volcanic rocks possessing geochemical features of typical OIB-type and HIMU-type basalts – the Zasur'ya enriched basalts (Fig. 13B). In Devonian time, the oceanic subduction of the PAO beneath the SW active margin of the Siberian continent resulted in the accretion of the seamounts to the Rudny Altai island arc (Fig. 13C). Later, the accretionary complex experienced tectonic deformation and strike-slip faulting as a result of continuing subduction and subsequent collision of the Altai-Mongolian microcontinent and Siberian continent (Buslov et al., 2000, 2001).

7. Conclusions

High-precision ICP-MS, SR XRF and INAA trace element data obtained from the Late Cambrian–Early Ordovician basaltic volcanic sequences of the Zasur'ya accretionary complex, which is a part of the Late Devonian Charysh-Terekta strike-slip zone, reveal con-

siderable geochemical diversity. Th–Nb–LREE-depleted, transitional and enriched basalts coexist in this geological structure.

The Zasur'ya depleted tholeiitic basalts have near-flat REE patterns, relatively high ε_{Nd} and multi-element spectra with dominantly negative Nb and Th anomalies, which are interpreted to stem from a shallow-deep mantle with recycled subduction influenced lithosphere. According to their geological association with deep-sea radiolarian cherts and geochemical data they were formed in a mid-oceanic ridge setting basalts and probably represent base of the Zasur'ya oceanic island/seamount.

The Zasur'ya transitional and enriched basalts are interpreted as liquids segregated from mantle plumes and erupted in an intraplate oceanic environment. Many of transitional basalts are compositionally similar to the lavas of the older seamounts of the Emperor-Hawaii Chain, which have less enriched LREE and similar Nb and Th anomalies from mixing of different mantle components. The enrichment of Nb with respect to La and Th, coupled with the medium ε_{Nd} values close to those in HIMU and the positively fractionated LREE patterns in transitional and enriched basalts is comparable with modern HIMU-type OIBs involving recycled oceanic crust in their mantle source. Negative to positive Zr (Hf) anomalies in these basalts suggest spinel to garnet facies depths of melt segregation in the mantle, i.e., below and above the 400 km level. Given the structural evidence for an accretionary complex setting, the plume from which the transitional and alkaline basalts were derived most probably erupted in an intra-oceanic environment far away from a Late Devonian collision zone.

Field relations suggest that all three types of basaltic sequences occur along the same tectonic zone, and have been laterally displaced by strike-slip faults. Accordingly, these mafic volcanic rocks, which are chemically diverse but occur within the same tectonostratigraphic unit, are likely fragments of Early Paleozoic (Late Cambrian) oceanic crust (oceanic floor) and oceanic islands/seamounts derived from a heterogeneous mantle plume. The diversity suggests that Late Neoproterozoic – Early Paleozoic subduction processes may have played an important role in the generation of chemically heterogeneous mantle.

Acknowledgements

Inna Safonova thanks Dr. Mikhail Buslov for fruitful discussions and encouragement, Dr. Olga Obut (IPGG SB RAS) for joint field works, and to Dr. Juyong Kim from KIGAM for assistance. Prof. Andy Saunders and an anonymous reviewer are acknowledged for their comments, which all were very useful. This paper could not have been produced without the skilful analytical work of V.A. Bobrov, A.D. Kireev, S.V. Palesskiy (IGM SB RAS, Novosibirsk). The work was partly supported by the RFBR-JSPS international grant no. 07-05-91211a. Inna Safonova was supported by the Korean Federation of Science and Technology (KOFST).

References

Arndt, N.T., Jenner, G.A., 1986. Crustally contaminated komatiites and basalts from Kambalda, Western Australia. Chemical Geology 56, 229–255.

Berzin, N.A., Dobretsov, N.L., 1994. Geodynamic evolution of Southern Siberia in Late Precambrian–Early Paleozoic time. In: Coleman, R.G. (Ed.), Reconstruction of the Paleo-Asian Ocean. Utrecht, The Netherlands, pp. 53–70.

Brenan, J.M., Shaw, H.F., Phinney, D.L., Ryerson, F.J., 1994. Rutile-aqueous fluid partitioning of Nb, Ta, Hf, Zr, U and Th: implications for high-field strength element depletions in island-arc basalts. Earth and Planetary Science Letters 128, 327–339.

Buslov, M.M., Berzin, N.A., Dobretsov, N.L., Simonov, V.A., 1993. Geology and Tectonics of Gorny Altai. UIGGM, Novosibirsk. p. 122.

Buslov, M.M., Saphonova, I.Yu., Bobrov, V.A., 1999. An exotic terrane of the Late Cambrian–Early Ordovician oceanic crust in the northwestern Gorny Altai (Zasurin Formation): structural position and geochemistry. Doklady Earth Sciences 368, 650–654.

Buslov, M.M., Fujiwara, Y., Safonova, I.Yu., Okada, Sh., Semakov, N.N., 2000. The junction zone of the Gorny Altai and Rudny Altai terranes: structure and evolution. Russian Geology and Geophysics 41, 377–390.

Buslov, M.M., Safonova, I.Yu., Watanabe, T., Obut, O., Fujiwara, Y., Iwata, K., Semakov, N.N., Sugai, Y., Smirnova, L.V., Kazansky, A.Yu., 2001. Evolution of the Paleo-Asian Ocean (Altai-Sayan region, Central Asia) and collision of possible Gondwana-derived terranes with the southern marginal part of the Siberian continent. Geosciences Journal 5, 203–224.

Buslov, M.M., Fujiwara, Y., Iwata, K., Semakov, N.N., 2004a. Late Paleozoic–Early Mesozoic geodynamics of Central Asia. Gondwana Research 7, 791–808.

Buslov, M.M., Watanabe, T., Fujiwara, Y., Iwata, K., Smirnova, L.V., Safonova, I.Yu., Semakov, N.N., Kiryanova, A.P., 2004b. Late Paleozoic faults of the Altai region, Central Asia: tectonic pattern and model of formation. Journal of Asian Earth Sciences 23, 655–671.

Chen, C.-Y., Frey, F.A., Garcia, M.O., Dalrymple, G.B., Hart, S.R., 1991. The tholeiitic to alkaline basalt transition at Heleakala volcano. Maui, Hawaii. Contributions to Mineralogy and Petrology 106, 183–200.

Didenko, A.N., Mossakovskiy, A.A., Pecherskiy, D.M., Ruzhentsev, S.G., Samygin, S.G., Kheraskova, T.N., 1994. Geodynamics of Paleozoic oceans of Central Asia. Russian Geology and Geophysics 35, 48–62.

Dobretsov, N.L., Berzin, N.A., Buslov, M.M., 1995. Opening and tectonic evolution of the Paleo-Asian Ocean. International Geology Review 35, 335–360.

Dobretsov, N.L., Buslov, M.M., Safonova, I.Yu., Kokh, D.A., 2004. Fragments of oceanic islands in the Kurai and Katun' accretionary wedges of Gorny Altai. Russian Geology and Geophysics 45, 1381–1403.

Floyd, P.A., 1989. Geochemical features of intra-plate oceanic plateau basalts. In: Saunders, A.D., Norry, M.J. (Eds.), Magmatism in the Ocean Basins, vol. 42. Special Publication of the Geological Society of London, pp. 215–230.

Fowler, A.D., Jensen, L.S., 1989. Quantitative trace element modeling of the crystallization history of the Kinojevis and Blake River groups, Abitibi greenstone belt, Ontario. Canadian Journal of Earth Sciences 26, 1356–1365.

Green, T.H., 1994. Experimental studies of trace-element partitioning applicable to igneous petrogenesis: Sedona 16 years later. Chemical Geology 117, 1–36.

Green, T.H., Sie, S.H., Ryan, C.G., Cousens, D.R., 1989. Proton microprobe-determined partitioning of Nb, Ta, Zr, Sr and Y between garnet, clinopyroxene and basaltic magma at high pressure and temperature. Chemical Geology 120, 347–359.

Hards, V.L., Kempton, P.D., Thompson, R.N., 1995. The heterogeneous Iceland plume: new insights from the alkaline basalts of the Snaefell volcanic centre. Journal of the Geological Society 152, 1003–1009.

Hemond, C., Arndt, N.T., Lichtenstein, U., Hofmann, A.W., Oskarsson, N., Steinthorsson, S., 1993. The heterogeneous Iceland plume: Nd–Sr–O isotope and trace element constrains. Journal of Geophysics Research 98, 15833–15850.

Hirschman, M.M., Stolper, E.M., 1996. A possible role for garnet pyroxenite in the origin of the "garnet signature" in MORB. Contributions to Mineralogy and Petrology 124, 185–208.

Hofmann, A.W., White, W.M., 1982. Mantle plumes from ancient oceanic crust. Earth and Planetary Science Letters 57, 421–436.

Hofmann, A.W., 1997. Mantle geochemistry: the message from oceanic volcanism. Nature 385, 219–229.

Humphris, S.E., 1984. The mobility of the rare earth elements in the crust. In: Henderson, P. (Ed.), Rare Earth Element Geochemistry. Elsevier, Amsterdam, pp. 317–342.

Ichiyama, Y., Ishiwatari, A., Koizumi, K., 2008. Petrogenesis of greenstones from the Mino-Tamba belt, SW Japan: evidence for an accreted Permian oceanic plateau. Lithos 100, 127–146.

Isozaki, Y., Maruyama, Sh., Fukuoka, F., 1990. Accreted oceanic materials in Japan. Tectonophysics 181, 179–205.

Isozaki, Y., Aoki, K., Nakama, T., Yanai, S., 2010. New insights into a subduction-related orogen: a reappraisal of the geotectonic framework and evolution of the Japanese Islands. Gondwana Research 18, 82–105.

Iwata, K., Sennikov, N.V., Buslov, M.M., Obut, O.T., Shokalsky, S.P., Kuznetsov, S.A., Ermikov, V.D., 1997. Upper Cambrian–Early Ordovician age of the Zasur'ia basalt-chert-terrigenous formation (northwestern Gorny Altai). Russian Geology and Geophysics 38, 1427–1444.

Jenner, G.A., Longerich, H.P., Jackson, S.E., Fryer, B.J., 1990. ICP-MS – a powerful tool for high precision trace element analysis in earth sciences: evidence from analysis of selected USGS. reference samples. Chemical Geology 83, 133–148.

Jensen, L.S., 1976. A new cation plot for classifying subalkalic volcanic rocks. Ontario Division Mines Misc.,vol. 66.

Jochum, K.P., Arndt, N.T., Hofmann, A.W., 1991. Nb–Th–La in komatiites and basalts: constraints on komatiites petrogenesis and mantle evolution. Earth and Planetary Science Letters 107, 272–289.

Jochum, K.P., Nohl, U., 2008. Reference materials in geochemistry and environmental research and the GeoReM database. Chemical Geology 253, 50–53.

Jones, D.L., Murchey, B., 1986. Geologic significance of Paleozoic and Mesozoic radiolarian chert. Annual Reviews in Earth and Planetary Science 14, 455–492.

Kamber, B.S., Collerson, K.D., 2000. Zr/Nb systematics of ocean island basalts reassessed – the case for binary mixing. Journal of Petrology 41, 1007–1021.

Kerr, A.C., White, R.V., Saunders, A.D., 2000. LIP reading: recognizing oceanic plateaus in the geological record. Journal of Petrology 41, 1041–1056.

Komiya, T., Maruyama, Sh., Hirata, T., Yurimoto, H., Nohda, S., 2004. Geochemistry of the oldest MORB and OIB in the Isua Supracrustal Belt. Southern West Greenland Implication for the composition and temperature of early Archean upper mantle. The Island Arc 13, 47–72.

Kurenkov, S.A., Didenko, A.N., Simonov, V.A., 2002. Geodynamics of paleospreading. GEOS, Moscow, p. 294 (in Russian).
Streckeisen, A., Zanettin, B., Le Bas, M.J., Bonin, B., Bateman, P., Bellieni, G., Dudek, A., Efremova, S., Keller, J., Lamere, J., Sabine, P.A., Schmid, R., Sorensen, H., Woolley, A.R., 2002. In: Le Maitre, R.W. (Ed.), Igneous Rocks: A Classification and Glossary of Terms, Recommendations of the International Union of Geological Sciences, Subcommission of the Systematics of Igneous Rocks. Cambridge University Press.
Mahoney, J.J., Storey, M., Duncan, R.A., Spencer, K.J., Pringle, M., 1993. Geochemistry and geochronology of Leg130 basement lavas: nature and origin of the Ontong Java Plateau. Proceedings of the Ocean Drilling Program, Scientific Results 130, 3–22.
Mahoney, J.J., Frei, R., Tejada, M.L., Mo, X.X., Leat, P.T., Nagler, T.F., 1998. Tracing the Indian Ocean mantle domain through time: isotopic results from old West Indian, East Tethyan, and South Pacific seafloor. Journal of Petrology 39, 1285–1306.
Maruyama, Sh., Isozaki, Yu., Kimura, G., Terabayashi, M., 1997. Paleogeographic maps of the Japanese Islands: plate tectonic synthesis from 750 Ma to the present. Island Arc 6, 121–142.
Maruyama, S., Santosh, M., Zhao, D., 2007. Superplume, supercontinent, and post-perovskite: Mantle dynamics and anti-plate tectonics on the Core–Mantle Boundary. Gondwana Research 11, 7–37.
McCulloch, M.T., Gamble, A.J., 1991. Geochemical and geodynamical constraints on subduction zone magmatism. Earth and Planetary Science Letters 102, 358–374.
Neal, C.R., Mahoney, J.J., Kroenke, L.W., Duncan, R.A., Petterson, M.G., 1997. The Ontong Java Plateau. In: Mahoney, J.J., Coffin, M.F. (Eds.), Large Igneous Provinces: Continental, Oceanic, and Planetary Flood Magmatism, vol. 100. American Geophysical Union Monograph, Washington, DC, pp. 183–216.
Orihashi, Y., Hirata, T., 2003. Rapid quantitative analysis of Y and REE abundances in XRF glass bead for selected GSJ reference rock standards using Nd-YAG 266 nm UV laser ablation ICP-MS. Geochemical Journal 37, 401–412.
Ota, T., Utsunomiya, A., Uchio, Yu., Isozaki, Y., Buslov, M., Ishikawa, A., Maruyama, Sh., Kitajima, K., Kaneko, Y., Yamamoto, H., Katayama, I., 2007. Geology of the Gorny Altai subduction–accretion complex, southern Siberia: tectonic evolution of a Vendian–Cambrian intra-oceanic arc. Journal of Asian Earth Sciences 30, 666–695.
Parsons, B., Sclater, J.G., 1977. An analysis of the variation of ocean floor bathymetry and heat flow with age. Journal of Geophysical Research 82, 803–827.
Phedorin, M.A., Bobrov, V.A., Chebykin, E.P., Goldberg, E.L., Melgunov, M.S., Filippova, S.V., Zolotarev, K.V., 2000. Comparison of synchrotron radiation X-ray fluorescence with conventional techniques for the analysis of sedimentary samples. Geostandards Newsletter: The Journal of Geostandards and Geoanalysis 24, 205–216.
Polat, Al., Kerrich, R., Wyman, D., 1999. Geochemical diversity in oceanic komatiites and basalts from the late Archean Wawa greenstone belts, Superior Province, Canada: trace element and Nd isotope evidence for a heterogeneous mantle. Precambrian Research 94, 139–173.
Putchel, I.S., Haase, K.M., Hofmann, A.W., Chauvel, C., Kulikov, V.S., Garbe-Schonberg, C.-D., Nemchin, A.A., 1997. Petrology and geochemistry of crustally contaminated komatiitic basalts from the Vetreny belt, southeastern Baltic shield: evidence for an early Proterozoic mantle plume beneath rifted Archean continental lithosphere. Geochimia et Cosmochimia Acta 61, 1205–1222.
Redman, B.A., Keays, R.R., 1985. Archean volcanism in the eastern Goldfields Province, Western Australia. Precambrian Research 30, 113–152.
Reid, I., Jackson, H.R., 1981. Oceanic spreading rate and crustal thickness. Marine Geophysical Researches 5, 165–172.
Regelous, M., Hofmann, A.W., Abouchami, W., Galer, S.J.G., 2003. Geochemistry of Lavas from the Emperor Seamounts, and the Geochemical evolution of Hawaiian Magmatism from 85 to 42 Ma. Journal of Petrology 44, 113–140.
Rojas-Agramonte, Y., Kröner, A., Demoux, A., Xia, X., Wang, W., Donskaya, T., Liu, D., Sun, M., in press. Detrital and Xenocrystic Zircon Ages from Neoproterozoic to Paleozoic Arc Terranes of Mongolia: Significance for the Origin of Crustal Fragments in the Central Asian Orogenic Belt. Gondwana Research, 10.1016/j.gr.2010.10.00.
Rollinson, H.R., 1993. Using Geochemical Data: Evaluation, Presentation, Interpretation. Longman Group UK Ltd.. 352 p.
Rudnick, R., Barth, M., Horn, I., McDonough, W.F., 2000. Rutile-bearing refractory eclogites: missing link between continents and depleted mantle. Science 287, 278–281.
Safonova, I.Yu., 2005. Vendian-Paleozoic basalts of the Paleo-Asian Ocean incorporated in foldbelts of Gorny Altai and East Kazakhstan: geodynamic settings of formation. Candidate of Sciences Thesis Autoreferate. NP AI «Geo», Novosibirsk, p. 20 (in Russian).
Safonova, I.Yu., 2008. Geochemical evolution of the Paleo-Asian Ocean intra-plate magmatism from the Late Neoproterozoic to the Early Cambrian. Petrology 16, 492–511.
Safonova, I.Yu., 2009. Intraplate magmatism and oceanic plate stratigraphy of the Paleo-Asian and Paleo-Pacific Oceans from 600 to 140 Ma. Ore Geology Reviews 35, 137–154.
Safonova, I.Yu., Buslov, M.M., Iwata, K., Kokh, D.A., 2004. Fragments of Vendian–Early Carboniferous oceanic crust of the Paleo-Asian Ocean in foldbelts of the Altai-Sayan region of Central Asia: geochemistry, biostratigraphy and structural setting. Gondwana Research 7, 771–790.
Safonova, I.Yu., Simonov, V.A., Buslov, M.M., Ota, T., Maruyama, Sh., 2008. Neoproterozoic basalts of the Paleo-Asian Ocean (Kurai accretion zone, Gorny Altai, Russia): geochemistry, petrogenesis, geodynamics. Russian Geology and Geophysics 49, 254–271.
Safonova, I.Yu., Utsunomiya, A., Kojima, S., Nakae, S., Tomurtogoo, O., Filippov, A.N., Koizumi, K., 2009. Pacific superplume-related oceanic basalts hosted by accretionary complexes of Central Asia, Russian Far East and Japan. Gondwana Research 16, 587–608.
Saunders, A.D., Norry, M.J., Tarney, J., 1988. Origin of MORB and chemically-depleted mantle reservoirs: trace element constrains. Journal of Petrology (Special Lithosphere Issue), 415–455.
Sengör, A.M.C., Natal'in, B.A., 1996. Palaeotectonics of Asia: fragments of a synthesis. In: Yin, A., Harrison, M. (Eds.), Tectonic Evolution of Asia. Cambridge University Press, Cambridge, pp. 486–640.
Sennikov, N.V., Iwata, K., Ermikov, V.D., Obut, O.T., Khlebnikova, T.V., 2003. Oceanic sedimentation settings and fauna associations in the Paleozoic on the southern framing of the West Siberian Plate. Russian Geology and Geophysics 44, 156–171.
Sennikov, N.V., Obut, O.T., Iwata, K., Khlebnikova, T.V., Ermikov, V.D., 2004. Lithological Markers and Bio-indicators of Deep-water Environments During Paleozoic Siliceous Sedimentation (Gorny Altai Segment of the Paleo-Asian Ocean). Gondwana Research 7, 843–852.
Silver, P.G., Carlson, R.W., Olson, P., 1988. Deep slabs, chemical heterogeneity, and structure of mantle convection: investigation of an enduring paradox. Annual Review of Earth and Planetary Sciences 16, 477–541.
Simonov, V.A., Dobretsov, N.L., Buslov, M.M., 1994. Boninite series in structures of the Paleo-Asian Ocean. Russian Geology and Geophysics 35, 182–199.
Simonova, V.I., Ivanova, L.D., Smertina, L.N., 1987. A comparative study of the schemes of geological sample preparation for flame atomic absorption analysis. Journal of Analytical Chemistry XLII, 224–231 (in Russian).
Stern, R.A., Syme, E.C., Lucas, S.B., 1995. Geochemistry of 1.9 Ga MORB- and OIB-like basalts from the Amisk collage, Fin Flon belt, Canada: evidence for an intraoceanic origin. Geochimia et Cosmochimia Acta 59, 3131–3154.
Sun, S., McDonough, W.F., 1989. Chemical and isotopic systematics of oceanic basalts: implications for mantle composition and processes. In: Saunders, A.D., Norry, M.J. (Eds.), Magmatism in the Ocean Basins. Geol. Soc., London, pp. 313–345 (Special Publication 42).
Taylor, S.T., McLennan, S.M., 1985. The Continental Crust: Composition and Evolution. Blackwell, Oxford. 312 pp.
Ueda, H., Kawamura, M., Niida, K., 2000. Accretion and tectonic erosion processes revealed by the mode of occurrence and geochemistry of greenstones in the Cretaceous accretionary complexes of the Idonappu zone, southern central Hokkaido, Japan. The Island Arc 9, 237–257.
Utsunomiya, A., Jahn, B.-m., Ota, T., Safonova, I.Yu., 2009. Geochemical and Sr–Nd isotopic study of the Vendian greenstones from Gorny Altai, southern Siberia: implications for the tectonic setting of the formation of greenstones and the role of oceanic plateau in accretionary orogen. Lithos 113, 437–453.
Wakita, K., 2000. Melanges of the Mino Terrane. Memoirs of the Geological Society of Japan 55, 145–163 (in Japanese with English abstract).
White, R.V., Tarney, J., Kerr, A.C., Saunders, A.D., Kempton, P.D., Pringle, M.S., Klaver, G.T., 1999. Modification of an oceanic plateau, Aruba, Dutch Caribbean: implications for the generation of continental crust. Lithos 46, 43–68.
Wilson, M., 1993. Geochemical signature of oceanic and continental basalts: a key to mantle dynamics. Journal of the Geological Society 150, 977–990.
Winchester, J.A., Floyd, P.A., 1977. Geochemical discrimination of different magma series and their differentiation products using immobile elements. Chemical Geology 20, 325–343.
Windley, B.F., Alexeiev, D., Xiao, W., Kroner, A., Badarch, G., 2007. Tectonic models for accretion of the Central Asian Orogenic Belt. Journal of the Geological Society of London 164, 31–47.
Wong, K., Sun, M., Zhao, G., Yuan, C., Xiao, W., 2010. Geochemical and geochronological studies of the Alegedayi Ophiolitic Complex and its implication for the evolution of the Chinese Altai. Gondwana Research 18, 438–454.
Xiao, W.J., Han, C., Yuan, C., Sun, M., Lin, S., Chen, H., Li, Z., Li, J., Sun, S., 2008. Middle Cambrian to Permian subduction-related accretionary orogenesis of Northern Xinjiang, NW China: implications for the tectonic evolution of central Asia. Journal of Asian Earth Sciences 32, 102–117.
Xiao, W.J., Huang, B., Han, C., Sun, S., Li, J., 2010. A review of the western part of the Altaids: a key to understanding the architecture of accretionary orogens. Gondwana Research 18, 253–273.
Yakubchuk, A.S., 2004. Architecture and mineral deposit settings of the Altaid orogenic collage: a revised model. Journal of Asian Earth Sciences 23, 761–779.
Yarmolyuk, V.V., Kovalenko, V.I., 2003. Deep geodynamics and mantle plumes: their role in the formation of the central Asian fold belt. Petrology 11, 504–531.
Zhang, Y., Liu, J., Guo, Z., 2010. Permian basaltic rocks in the Tarim basin, NW China: implications for plume–lithosphere interaction. Gondwana Research 18, 596–610.
Zi, J., Fan, W., Wang, Yu., Peng, T., Guo, F., 2008. Geochemistry and petrogenesis of the Permian mafic dykes in the Panxi region, SW China. Gondwana Research 14, 368–382.
Zindler, A., Hart, S., 1986. Chemical geodynamics. Annual Reviews in Earth and Planetary Science 14, 493–571.
Zonenshain, L.P., Kuzmin, M.I., Natapov, L.M., 1990. Geology of the USSR: A Plate Tectonic Synthesis. Geodynamic Monograph, American Geophysical Union, Washington. 242p.